Adipose tissue macrophages develop from bone marrow-independent progenitors in *Xenopus laevis* and mouse

Syed F. Hassnain Waqas*[1], Anna Noble[†1], Anh C. Hoang*, Grace Ampem*, Manuela Popp*, Sarah Strauß[‡], Matthew Guille[†], Tamás Röszer*[2]

* Institute of Comparative Molecular Endocrinology, University of Ulm, Germany

[†] European *Xenopus* Resource Centre, School of Biological Sciences, University of Portsmouth, UK

[‡] Ambystoma Mexicanum Bioregeneration Center, Department of Plastic, Aesthetic, Hand and Reconstructive Surgery, Hannover Medical School, Medizinische Hochschule Hannover, Germany

Amphibian adipose tissue contains self-renewing macrophages that develop before the establishment of bone marrow hematopoiesis, and this mechanism is conserved in mouse.

[1] These authors contributed equally.

[2] Correspondence should be addressed to Tamás Röszer. Institute of Comparative Molecular Endocrinology, Center of Biomedical Research, University of Ulm, Science Park I, 89081 Helmholtzstrasse 8.1, Ulm, Germany; Tel.: +49 731 50 32630, e-mail: tamas.roeszer@uni-ulm.de

Short title: Developmental origin of adipose tissue macrophages

Abstract

Adipose tissue macrophages (ATMs) have a metabolic impact in mammals as they contribute to metabolically harmful adipose tissue (AT) inflammation. The control of ATM number may have therapeutic potential; however, information on ATM ontogeny is scarce. While it is thought that ATMs develop from circulating monocytes, various tissue-resident macrophages are capable of self-renewal and develop from bone marrow (BM)-independent progenitors, without a monocyte intermediate. Here we show that amphibian AT contains self-renewing ATMs that populate the AT before the establishment of BM hematopoiesis. *Xenopus* ATMs develop from progenitors of the anterior ventral blood island (aVBI). In the mouse, a significant amount of ATMs develop from the yolk sac, the mammalian equivalent of the aVBI. In summary, this study provides evidence for a prenatal origin of ATMs and shows that the study of amphibian ATMs can enhance the understanding of the role of the prenatal environment in ATM development.

Key words: fat body, yolk sac macrophages, CX_3CR1, *lurp*, neuropeptide FF

Introduction

Adipose tissue macrophages (ATMs) are resident macrophages of adipose tissue (AT) in mammals [1]. They have a largely unexplored role in AT immunity [2], and a better understood impact on metabolism [1]. ATMs can support normal AT function, but can also trigger AT inflammation, insulin resistance (IR) and, correspondingly, contribute to the development of obesity comorbidities [1-4]. Because ATMs are associated with the rising prevalence of obesity and its comorbidities [1, 3-5], they are of great pathophysiological relevance.

The quantity and the so-called activation state of ATMs are the two main determinants of their metabolic effects [1, 2]. Obesity increases the number of ATMs because of increased monocyte infiltration and local ATM proliferation in AT [1, 6, 7]. The increase in ATM content in obesity is associated with an inflammatory ATM phenotype, which is the result of classical or M1 macrophage activation [1, 2]. M1 activation of ATMs is promoted by modified lipids, lipoproteins and cytokines of the obese AT. M1-ATMs exacerbate AT inflammation, which can lead to IR [1-4]. By contrast, lean AT is rich in alternatively-activated, so-called M2 ATMs, which are thought to support homeostatic AT functions [1]. Inhibiting M1 activation and maintaining a metabolically-healthy M2-dominant ATM population is a therapeutic strategy in obesity and IR treatment [1, 2, 8]. Whether ATMs of lean AT develop from blood monocytes or are replenished by local proliferation of ATMs is unknown [2]. Since macrophages are present in almost all organs, pharmacological manipulation of macrophage activation and proliferation can have beneficial effects in AT; however, this can have detrimental effects in other tissues. To avoid such off-target effects, recent research efforts have focused on the identification of developmental programs and marker proteins that are specific for individual tissue-resident macrophages [9-12]. Such an approach could allow targeted manipulation, for example, drug delivery to specific macrophage niches. Therefore, a better understanding of ontogeny of ATMs can help in the development of methods to specifically increase the production of M2-ATMs without

affecting other tissue-resident macrophages. Nevertheless, in contrast to other tissue-resident macrophages, such as microglia, Kupffer cells or osteoclasts, to date little is known about the developmental program of ATMs [2].

Comparative studies facilitate the understanding of the development of specific cell types and may provide evidence of the evolutionary origin of ATMs. In this study, we show that ATMs are present in the African clawed frog *Xenopus laevis*, a widely-used model of vertebrate development. *Xenopus* ATMs develop from progenitors of the extraembryonic anterior ventral blood island (aVBI) and have the ability to proliferate. The aVBI is the equivalent of the hematopoietic tissue of the mammalian yolk sac (YS). Accordingly, we found that YS macrophages give rise to ATMs in the mouse.

Results

Visceral adipose tissue of *Xenopus laevis* is rich in macrophages

Amphibians were the first vertebrates to evolve and develop visceral white AT (WAT) [13]. The WAT is present in the abdominal cavity, forming paired fat bodies (Figure 1A). Whether macrophages are associated with amphibian WAT is unknown. Histological assessment of *Xenopus* fat bodies revealed WAT rich in stromal cells (SCs) (Figure 1B), with the majority exhibiting strong acid phosphatase (ACP) and peroxidase (POD) activity (Figure 1C). Both enzymes are associated with phagosomes and are expressed by amphibian macrophages [14, 15]. Using transmission electron microscopy (TEM) to examine the structure of sorted cells from WAT stroma, we identified cells with the typical morphology of *Xenopus* macrophages [16] (Figure 1C,D,J, Supplemental Figure 1A–C), and which expressed the macrophage marker Ly-6/uPAR-related protein-1 (lurp) (Supplemental Figure 1D). Furthermore, phagocytosis activity was restricted to macrophages of the WAT stroma (Figure 1E–H, Supplemental Video File), supporting the notion that analogous to mammalian WAT, amphibian WAT is infiltrated by ATMs.

Macrophage activation in amphibians remains poorly understood, and it is not known whether homologous mechanisms of M1 and M2 macrophage polarization exist [17]. It has been reported, however, that a NO-producing, pathogen killing, activation state of *Xenopus* macrophages can be elicited *in vitro* by polyinosine polycytidylic acid (pI:pC) and to a lesser extent by lipopolysaccharide (LPS) [17], which is reminiscent of the M1 activation of mammalian macrophages. To question whether *Xenopus* ATMs can adopt an M1-like activation state, we challenged *Xenopus* ATMs *in vitro* either with pI:pC for 4 h or with LPS for 6 h and 18 h and measured the transcription of genes encoding inflammatory mediators and receptors known to initiate pathogen clearance in *Xenopus*. These genes include *nos2* and *ifng* (interferon γ), which are produced by *Xenopus* macrophages in response to viral and bacterial infection [18, 19], and *mif* (macrophage inhibitory factor-1), which is linked to the

activation of leukocyte migration in *Xenopus* [20]. We found that pI:pC treatment increased *nos2* and *mif* transcription (Supplemental Figure 1E). Of note, *Xenopus* ATMs were relatively insensitive to LPS treatment, which is in agreeement with data from amphibian macrophages [21]. Accordingly, prolonged (18 h) LPS exposure, but not short-term (6 h) exposure, increased the transcription of *csf1* (colony stimulating factor-1), *csf1r* (csf-1 receptor), *ifng* and *mif*, whereas *tgfb* (transforming growth factor-β) transcription remained unchanged (Supplemental Figure 1F). CSF1 may polarize *Xenopus* macrophages towards a NOS2-expressing, hence M1-like activation state [17]. Though amphibians have toll-like receptors (TLRs) and notwithstanding that TLR signaling ensures pathogen recognition and activation of the innate immune response, recognition of LPS is weak in amphibians, possibly due to the absence of TLR4 [21]. Collectively, the results show that *Xenopus* WAT contains immune competent ATMs that can adopt an M1-like activation state in response to pathogen-associated signals (Figure 1A–J, Supplemental Figure 1A–F).

Xenopus ATMs can self-renew

In addition to their activation state, increased ATM proliferation contributes to the metabolic dysfunction of obese WAT in mammals [6, 22]. To determine whether *Xenopus* ATMs had proliferative capacity, SCs of the WAT were isolated and labeled *in vitro* with bromo-deoxyuridine (BrdU). We observed that BrdU incorporation was present only in ATMs (Figure 2A–C). Because false-positive staining may occur in phagocytosing cells engulfing BrdU-labeled cells, we confirmed that the ATMs were able proliferate by culturing them for 24–72 h in soft agar and monitoring their ability to grow as colonies. As observed by differential interference contrast microscopy, the resulting colonies displayed a morphology resembling that of *Xenopus* hematopoietic colonies (Figure 2D) [23], and TEM analysis confirmed leukocyte morphology (Figure 2E).

Given the ability of *Xenopus* ATMs to proliferate and form colonies, we next asked whether WAT contains hematopoietic progenitors. The expression level of *scl* (stem cell

leukemia), a key transcription factor of amphibian hemangioblast development and hematopoiesis [24, 25], in SCs of WAT was compared with that in the hematopoietic organs liver, spleen and bone marrow (BM). Spleen and liver had the highest levels of *scl* transcription in adult *Xenopus* (Figure 3A), whereas BM, which makes only a minor contribution to hematopoiesis in adult amphibians, had negligible expression. SCs of the WAT had comparable *scl* levels with those of spleen and liver (Figure 3A). The presence of scl^+ cells in WAT was confirmed by histology and FACS analysis of transgenic *scl*:eGFP *Xenopus* fat bodies (Figure 3B, scl^+ cells in spleen and liver are shown in Supplemental Figure 2).

During amphibian embryogenesis, the first wave of macrophages develops from $lurp^+$ precursors, which also show *scl* expression and have the ability to proliferate [24]. $Lurp^+$ myeloid cell precursors occur first in the aVBI in the early tailbud embryo [24], the so-called extraembryonic compartment of hematopoiesis that corresponds to the mammalian yolk sac (YS) hematopoietic tissue [26]. The aVBI develops into the vitelline veins, which contribute to the formation of the liver sinusoids [26], and thus may allow the colonization of the developing liver with $lurp^+$ cells. Accordingly, we detected *lurp* transcription in the adult liver and also in the spleen (Figure 3C). Additionally, BM displayed a comparable level of *lurp* transcription (Figure 3C), conceivably due to its ability to generate myeloid cells in the *Xenopus* adult [27].

While it has been shown that $lurp^+$ macrophage precursors of the aVBI proliferate and infiltrate tissues before the development of the circulatory system [24], it is not known whether they reach WAT. We found that *lurp* transcription was higher in the adult SCs of the WAT than in tested hematopoietic organs (Figure 3C), suggesting that it is rich in $lurp^+$ macrophage progenitors. The presence of $lurp^+$ cells was confirmed in the stroma by FACS analysis of transgenic *lurp*:eGFP *Xenopus* (Figure 3D, Supplemental Figure 2) [24]. Expression of *lurp* in the WAT was restricted to the ATM population as shown by FACS

analysis (Supplemental Figure 1D). Collectively these findings strongly suggest that *Xenopus laevis* fat bodies contain a self-renewing population of ATMs.

Xenopus ATMs settle in WAT before development of bone marrow

We next investigated at what stage in ontogeny ATMs emerge in the WAT. We detected fat bodies in *Xenopus* embryos from stage 60 onwards (Supplemental Figure 3A), a period during which hematopoiesis takes place in the liver and kidney. $Lurp^+$ ATMs were also detected from stage 60 (Figure 3E). Infiltration of the WAT by $lurp^+$ ATMs was concomitant with the development of BM-independent hematopoiesis. Indeed, WAT and ATM development preceded the development of the BM (Supplemental Figure 3A,B). Although BM of *Xenopus* can generate leukocytes [27], ACP^+ BM macrophages were detected only in adults, where macrophages were associated with fat cells (Supplemental Figure 3C).

As a robust test to determine whether ATMs could be generated in the complete absence of BM hematopoiesis, we took advantage of the fact that the axolotl, *Ambystoma mexicanum*, lacks BM hematopoietic progenitors [28]. Liver and spleen are responsible for definitive hematopoiesis in the axolotl in place of the BM [28]. In axolotl WAT, we could identify ACP^+ ATMs (Figure 3F,G), indicating that hepatic and splenic hematopoiesis could generate ATMs. Collectively, these findings show that amphibian WAT is colonized by BM-independent macrophage precursors, and ATMs exist despite the complete lack of BM hematopoiesis.

Xenopus and mouse share a homologous mechanism of ATM development

Xenopus embryonic development shares many features with mammalian embryogenesis. The functional equivalent of the aVBI in mammals and birds is the YS [26], and YS-derived macrophages give rise to tissue-resident macrophages in birds [29]. Moreover, it has been recently shown that YS-derived macrophage progenitors contribute to various tissue-resident macrophage populations in the mouse, such as microglia, cardiac resident macrophages and

arterial macrophages [10, 11, 30, 31]. In mammals, the first wave of YS macrophages has a maternal origin, and these cells persist between embryonic (E) day 7.5 and 9.5. From E8, the YS produces a second wave of macrophages that is characterized by four developmental stages with specific cell surface expression of antigens (Supplemental Table 1). We found that ATMs of the adult mouse WAT share similarities in cell surface pattern with YS macrophages, such as their $CD45^{+}$, Kit^{low}, $F4/80^{+}$, $MCSFR(CD115)^{+}$ and CX_3CR1^{bright} profile (Figure 4A–F). The majority of ATMs was CX_3CR1^{bright}, both after birth and in adulthood (Figure 4G). The so-called stage 4 YS macrophages proliferate, give rise to some tissue-resident macrophages and persist into adulthood [10, 11, 30-34]. Further, stage 4 YS-derived macrophage progenitors can be identified by the early onset expression of the chemokine receptor CX_3CR1, allowing them to be tracked from E9 onwards [10, 11, 30-34].

We evaluated whether a homologous mechanism of BM-independent ATM development was operating in the mouse. We used a tamoxifen-inducible eGFP model to label CX_3CR1^{+} stage 4 YS macrophage progenitors at E9 (Figure 4H), and we analyzed the fat depots after birth. In mouse, the brown AT (BAT) develops before birth [35]; hence, we first examined the interscapular BAT 7 days after birth. While we could not identify significant amounts of ATMs within the BAT stroma (Supplemental Figure 4), other myeloid cells, such as granulocytes and mast cells, were abundant (Supplemental Figure 4). Next, we analyzed the inguinal fat depot (iWAT), which starts to expand at birth [35]. Notably, we found that the majority of ATMs were $eGFP^{+}$ at adulthood (Figure 4I), indicating that YS-derived ATMs persist in iWAT after birth. Moreover, we detected a similar amount of $Ki67^{+}$ ATMs after birth and in adulthood (Figure 4J), showing that ATMs proliferate locally. These findings demonstrate that mouse ATMs have a YS origin and retain the ability of proliferation. This is in accordance with our recent report, showing that ATMs are capable of self-renewal without the need for monocyte supply, and that proliferating ATMs in mouse express CX_3CR1 [36]. Further, when we transplanted lineage negative $CD45.2^{+}$ BM

progenitors into lethally irradiated CD45.1^{+} mice, we found that the majority of the ATMs remained CD45.1^{+} in the recipients (Figure 4J).

Taken together, these data show that similar to *Xenopus laevis*, ATMs in the mouse have a BM-independent origin with potential for self-renewal (Figure 4K,L).

ATM development and activation in *Xenopus laevis* is controlled by gpr147

Recent findings suggest that M2-activating cytokines allow macrophage self-renewal [37]; however, it is unknown whether M2 macrophage activation occurs in vertebrates other than mammals. We thus sought to define whether *Xenopus* ATMs can polarize towards an M2-equivalent activation state, and also whether this can increase ATM proliferation. Under physiological conditions, M2 ATM activation is maintained by various tissue factors in mammals such as neuro-hormonal signals of fat metabolism [38]. While searching for hormone receptors that have abundant transcription in the *Xenopus* fat body, we identified *gpr147* as being specifically and highly expressed in the WAT stroma of adult *Xenopus* (Figure 5A). The *Xenopus gpr147* encodes a putative G-protein coupled receptor, which is a homolog of the mammalian neuropeptide FF (NPFF) receptor and thus *gpr147* is also called *npffr1*. The ligand for NPFF receptors, NPFF, is an evolutionarily conserved neuropeptide of deuterostomes [39] that has been shown to inhibit adipogenesis [40] and has a plausible role in macrophage activation in mammals [41]. Indeed, neuropeptides have an impact on immune cell functions in *Xenopus* [42] and macrophage activation in mammals [43]. Given this information, we analyzed the effect of gpr147 on *Xenopus* ATM development. When we ablated *gpr147* in *Xenopus*, the first (F0) generation gpr147-knockout (gpr147-KO) animals presented a reduction in *lurp* transcription in the WAT concomitant with a reduction in ATM content (Figure 5B–D).

To test whether NPFF has an impact on *Xenopus* ATM content and activation, we treated ATMs with NPFF (1 nM) *in vitro*, and found that NPFF-treated ATMs formed larger colonies in soft agar than vehicle-treated ATMs (Figure 5E,F). Moreover, when gpr147-KO

ATMs were compared with wild-type ATMs, the level of expression of *nos2* and *il34* (encoding interleukin-34; IL-34) was significantly higher and lower, respectively, in gpr147-KO cells (Figure 5G). Furthermore, NPFF-treated wild-type ATMs displayed increased transcription of the pro-resolving and pro-fibrotic genes, *tgfb* and *arg1* (arginase-1) (Figure 5H); both are hallmarks of M2 activation in mammalian macrophages [38]. In non-mammalian vertebrates, arginase-1 and TGF-β are associated with tissue healing and resolution of inflammation [38], pointing to a possible role for NPFF in M2 activation in *Xenopus* ATMs. Additionally, administration of NPFF increased the transcription of *il34* (Figure 5H). It has been shown recently that *Xenopus* IL-34 induces a unique activation state of *Xenopus* macrophages that is characterized by prominent *arg1* expression [44]. NPFF also suppressed the expression of the inflammatory genes *nos2* and *mif* (Figure 5H). In murine macrophages, the M1 activation state is typified by *NOS2* expression and NO synthesis, while M2 activation is characterized by increased arginase-1 expression and the abolishment of NO synthesis [38]. As a homolog of this model, our data support the notion that pI:pC- or LPS-stimulated *Xenopus* macrophages can be assigned as M1-macrophages, and NPFF-treated macrophages as M2-macrophages. Deficiency for gpr147 increased the transcription of *rnf128*, while NPFF treatment had the opposite effect (Figure 5I). *Xenopus rnf128* is a homolog of the mammalian *Rnf128* or *Grail*, which encodes an E3 ubiquitin ligase that increases the proteasomal degradation of phosphorylated STAT-6, the major signal transducer of M2 activation in mammals [45]. NPFF also inhibited pI:pC-induced transcriptional changes in ATMs (Figure 5J).

It is known that NPFF is expressed in the amphibian brain [46]. In addition, we screened for NPFF expression in the endocrine organs and found that only pancreas had a notable NPFF content. Accordingly, NPFF-like immunoreactvity was present in endocrine cells of the pancreas, which were scattered in the exocrine parenchyme (Supplemental Figure 5). The source of NPFF may therefore be either the central nervous system or the pancreatic endocrine cells.

Discussion

ATMs have a key metabolic impact in mice and primates [2]; however, an evolutionarily understanding of their equivalents and developmental origin is lacking. We have previously shown that ATMs are present in all relevant taxa of mammals [47]. While the majority of investigation with ATMs is centered on murine models of human obesity, some recent studies confirm that ATMs have a general metabolic and endocrine function in mammals [47-49]. In the present study, we show that ATMs are present in amphibian (*Xenopus laevis and Ambystoma mexicanum*) WAT, suggesting that they are evolutionarily conserved constituents of the WAT immune cell population in vertebrates.

Both amphibian and mammalian innate immune systems use macrophages as a first line of defense against cellular and viral pathogens [16, 17, 21]; however, several key mechanisms remain to be defined in the development and function of the amphibian immune system [21]. Indeed, while the immune system of *Xenopus* is the most comprehensively studied outside mammals and chicken [21], the functions and the development of *Xenopus* tissue-resident macrophages are relatively unknown. Macrophages are key for tissue regeneration in mammals [50], and studies using the axolotl *Ambystoma* mexicanum show that macrophages are also crucial for tissue healing in this highly regenerative species [51-53]. However, the axolotl hematopoietic system has only recently been explored [28] and information on tissue resident macrophages in *Ambystoma* remains scarce in the literature [54-57]. Whereas some studies have shown that the amphibian liver contains phagocytosing macrophages, which may be the equivalent of mammalian Kupffer cells [14, 58], these macrophages synthesize and degrade melanin, and are therefore very different to Kupffer cells [14, 55]. Phagocytosing astrocytes and microglia are also present in amphibians, with a role in myelin remodeling and nerve injury regeneration [59, 60]. Moreover, bone resorbing cells in amphibians are thought to be homologs of mammalian osteoclasts [61], or odontoclasts [62]. It remains to be established whether amphibians have the equivalents of mammalian type cardiac and intimal macrophages, and other types of tissue-resident macrophages. Indeed, it

has been shown that amphibians lack specialized populations of leukocytes in tissues, and they also lack lymph nodes, tonsils and Peyer-plaques within mucosal layers [21, 63]. Our study identifies a novel accumulation site of leukocytes in the periphery, and shows that WAT hosts a leukocyte niche formed by lymphocytes and ATMs. To our knowledge, this is the first report showing the existence of ATMs in non-mammalian vertebrates.

Xenopus laevis and *Ambystoma mexicanum* are important model organisms in comparative studies of immunity, development and regeneration [21, 64, 65], and it is therefore interesting that both species harbor ATMs in their fat depots. Moreover, *Ambystoma mexicanum* is a critically endangered species [66], and data on axolotl physiology therefore has high value for research. The evolutionarily and genetic distance of amphibians from mammals allows recognition of those features of the immune system that are resistant to evolutionarily change. In human and mouse, accumulation of ATMs was initially observed in a disease context and was considered a pathological consequence of obesity [1, 2]. Nevertheless, our present and previous findings [47] show that the association of WAT and leukocytes, specifically ATMs, is a conserved trait of vertebrates. Though WAT is not exposed to the environment, blood circulation from the intestine can deliver pathogen-associated signals to the WAT, which can elicit an innate immune response of ATMs. The close association of *Xenopus* ATMs with lymphocytes makes communication between these cells feasible, and may be the evolutionarily root of mammalian AT immune function.

While macrophages were traditionally viewed as terminally differentiated monocytes lacking the capacity for proliferation and self-renewal [67], recent data challenge this view. It has been shown that monocyte recruitment into tissues is not the only possible source of tissue macrophages. Indeed, microglia, liver Kupffer cells, arterial and cardiac macrophages have been shown to develop without monocyte intermediates [11, 30]. Kupffer cells are replenished by a locally proliferating macrophage progenitor pool [9], and microglia, arterial and cardiac macrophages originate, at least partially, from self-renewing macrophages of the embryonic YS [10, 30]. These findings suggest that tissue resident macrophages can locally

proliferate [9], thus allowing replenishment of the tissue-specific macrophage pool. While the ontogeny of the majority of the tissue-resident macrophages has been explored in mammals, information is lacking for the origin of ATMs [2]. In obesity, ATMs are derived from circulating monocytes [7], but can also be produced by local proliferation of ATMs [6]. Indeed, we have shown recently that ATMs can self-renew in lean AT in mouse [36]. ATM-specific delivery of anti-inflammatory drugs is a potential therapeutic approach for the targeted resolution of AT inflammation, without inducing an unwanted general immunosuppression. The lack of information on the origin of ATMs [2], however, impedes the development of tools which can selectively target ATMs. Comparative studies like ours are therefore important to better understand the developmental program of ATMs. In the present study, we show that *Xenopus* ATMs are derived from myeloid cell progenitors of the aVBI and populate the developing AT before the establishment of the BM.

The developmental origin of tissue macrophages in amphibians has been poorly investigated [24, 68]. Because the *Xenopus* embryo is exposed to the environment, its innate immune system develops rapidly, and macrophage progenitors appear 22–23 h post fertilization [21]. They invade peripheral tissues before the onset of the circulatory system [69] and exhibit *lurp* expression [24]. A recent study has described lurp$^-$ macrophages in *Xenopus* [65], which may develop from a yet undefined myeloid lineage. As we show herein, ATMs express *lurp*, indicating their origin to be aVBI progenitors. ATMs are present throughout the larval stage, metamorphosis and adulthood, despite the distinct hematopoietic organs of these developmental stages. This indicates that ATM number is not affected by the change in the site of hematopoiesis or by the remodeling and down-regulation of immune function that normally occurs in metamorphosis [21]. This may be a consequence of the ability of ATMs to proliferate locally and therefore to replenish the ATM pool without the need for a hematopoietic organ. ATMs were also detected in the axolotl *Ambystoma*, which lacks BM myeloid progenitors, further confirming that early larval hematopoiesis is sufficient to generate ATM progenitors and ATMs can develop in species that lack BM hematopoiesis.

However, the hematopoietic potential of the fat body is limited, as shown by the lack of erythropoiesis from fat body stromal cells, and the low number of *scl*-expressing cells in the AT stroma. We also show that ATM number and activation state is controlled by a neuropeptide in *Xenopus*. This further confirms that ATM development is a controlled physiological process, rather than a passive and uncontrolled accumulation of macrophages as is currently considered [2].

We found that the YS, the mammalian equivalent of the aVBI, contributes to the ATM pool in mouse. A BM contribution to the generation of ATMs has been documented in obese mice [70] and BM-derived progenitors can give rise to phagocytic cells, which resemble adipocyte morphology but express macrophage markers [71]. Interestingly, whole-body irradiation followed by BM transplantation impedes the expansion of AT in genetically obese (*ob/ob*) mice and reduces AT transcription of *Mcp1*. These effects are thought to reduce monocyte recruitment into AT, thus decreasing ATM number [72]. However, ATM content is not decreased following BM transplantation in *ob/ob* mice [72]. Moreover, ATM-associated metabolic effects of some nuclear receptors are not transmitted with BM transplantation [73]. These observations may be understood as signs of the existence of BM-independent maintenance of ATM content. We also show in our study that BM can contribute to ATM replenishment after BM transplantation, however, BM-derived ATMs represent the minority of the ATM content in mouse. Overall, our present findings together with a recent study by us [36] establish the existence of a BM-independent replenishment of ATMs. We also show that the majority of ATMs have a YS origin in lean AT in mouse. Importantly, the prenatal development of ATM progenitors raises the possibility that maternal factors can have an impact on ATM number and activation state. Currently, much attention is paid to the effect of the prenatal environment on the risk for inflammatory diseases and metabolism in adulthood [74]. Maternal nutrition, inflammatory status, infections and bioactive factors of the maternal blood all can have late-acting effects on immunity and metabolism [74]. Macrophage number and activation state are influenced by nutrition, and by inflammatory mediators and bioactive

371 factors such as hormones and vitamins. It is feasible that these factors are also operative in the
372 prenatal environment, although there are significant gaps in our understanding of prenatal
373 macrophage functions [75, 76]. Since the *Xenopus* embryo develops externally, development
374 of amphibian ATMs occurs without maternal influence, making *Xenopus* a tractable model
375 system of ATM development *via* exposure to various inflammatory signals, hormones and
376 other bioactive factors.

377 The use of *Xenopus* as a model of ATM development has an additional advantage over
378 mouse models because myeloid precursors are anatomically separated from erythroid and
379 lymphoid progenitors in the early tailbud embryo [24, 69]. Although appropriate markers to
380 distinguish the hematopoietic lineages in *Xenopus* by FACS analysis are lacking, this
381 anatomical separation allows targeted manipulation of the early myeloid lineage and the
382 identification of determinants of ATM development, which can lead to specific approaches
383 targeting ATM development without adverse off-target effects on other tissue macrophages.

384 In summary, our study shows that the evolutionary history of WAT is shared with
385 ATMs. Due to the conservation of fundamental mechanisms of immunity between
386 amphibians and mammals, exploring the features of amphibian ATM development will not
387 only enhance the understanding of the amphibian immune response *per se*, but will also aid in
388 the understanding of the impact of ATM development on organ homeostasis and metabolism.

Acknowledgements

This study was supported by the European Commission Horizon 2020 Research and Innovation Program, Marie-Curie-Skłodowska Individual Fellowship (655598, to T.R.), the German Research Fund DFG (RO 4856/1-1 to T.R.), the German Academic Exchange Service DAAD (to S.F.H.W.), and the Department of Comparative Molecular Endocrinology (Director, Prof. Dr. Jan Tuckermann). The work at the EXRC was funded by the Wellcome Trust (101480Z to MG). The authors thank the laboratory of Prof. Dr. Michael Kühl (University of Ulm) for providing *Xenopus laevis* tissues, the laboratory of Prof. Dr. Hartmut Geiger (Gina Moira Marka and Desirée Schütz), University of Ulm, for providing tissues of CD45.1/CD45.2 chimeric mice, Susanne Schmidt for her technical help, Dreamstime Stock Photography for providing the illustration of an adult *Ambystoma mexicanum* shown in Figure 3F, and Dr. Kenneth McCreath for critical reading of the manuscript.

Materials and Methods

Xenopus laevis and *Ambystoma mexicanum* strains

For assays on adult *Xenopus laevis* fat bodies, we used specimens from wild-type female frogs and *lurp*:eGFP (*Xla.Tg(slurp1l:GFP)*^{1Mohun} or *scl*:eGFP (European *Xenopus* Resource Centre, Portsmouth, UK) transgenic frogs at age 1–2 years. Animals were maintained according to general protocols [77]. For developmental studies, *lurp*:eGFP embryos were cultured and staged as described previously [77, 78]. Fat body specimens of *Ambystoma mexicanum* were obtained from wild-type adult females (Internal MHH file reference: 2012/2, donor animals according §4 TierSchG) bred and housed at Ambystoma Mexicanum Bioregeneration Center (Hannover, Germany), as previously described [79].

Manipulation of *Xenopus laevis* embryos

All animal work at the European *Xenopus* Resource Centre (EXRC, Portsmouth, UK) was approved by the Animal Welfare Ethical Review Board of the University of Portsmouth and carried out under the appropriate Home Office licence. *Xenopus laevis* were obtained from the EXRC, maintained at 18^{o}C on a daily light-dark cycle 13–11 h, and fed daily with Horizon XP pellets. Wild-type *Xenopus laevis* eggs were obtained by injecting 400 IU of human chorionic gonadotrophin into the dorsal lymph sacs of adult females on the evening before egg collection. Eggs were fertilized *in vitro* with macerated testes, dejellied with 2% cysteine hydrochloride (pH 7.8–8.0) and cultured in 0.1× modified Barth´s solution. Staging of *Xenopus laevis* embryos was done according to Nieuwkoop and Faber [78]. Cas9 mRNA (2 ng/embryo) and sgRNA (each 400 pg/embryo) was injected into the animal pole of one-cell stage embryos [80].

Generation of *Cas9* mRNA and gRNAs

Cas9 mRNA and sgRNAs were generated as described [81]. The oligonucleotides used to prepare sgRNA templates are listed in Supplemental Table 2. We used the online tool http://www.crisprscan.org/ to design the 5' oligonucleotides of sgRNAs. For sgRNA transcription, DNA templates were obtained by PCR assembly (forward primer: Supplemental Table 4, and reverse primer: 5'-AAAAGCACCGACTCGGTGCCACTTTTTCAA-GTTGATAACGGACTAGCCTTATTTTAACTTGCTATTTCTAGCTCTAAAAC-3'). The amplicons were transcribed with the MEGAshortscript® T7 Transcription Kit (Invitrogen, Carlsbad, California, USA) followed by DNAse digestion, and transcripts were purified with SigmaSpin^{TM} Sequencing Reaction Clean-Up columns (Sigma-Aldrich, St. Louis, Missouri, USA). Cas9 mRNA was produced using the mMessage mMachine Kit SP6 (Invitrogen, Carlsbad, California, USA) from a modified Cas9 construct in pCS2 (Supplemental Figure 6).

Evaluation of gene targeting efficiency in sgRNA/Cas9-injected *X. laevis* embryos

The targeting efficiency was examined at stage 32. We randomly collected five healthy embryos from each injection, extracted genomic DNA using the DNeasy Blood & Tissue Kit (Qiagen, Hilden, Germany) and amplified the targeted region by PCR (for primers see Supplemental Table 3). We performed a standard T7 endonuclease I assay to detect Cas9 induced mutations.

Detection of YS-derived ATMs in mouse

To label YS-derived macrophages, we adapted the lineage tracing protocol described elsewhere [11, 30]. Briefly, we crossed the Cx3cr1$^{tm21.(cre/ERT2)Jung}$ (The Jackson Laboratory, Bar Harbor, Maine, USA) mouse line, which carries a tamoxifen inducible Cre recombinase under the control of the Cx3cr1 promoter, with the Gt(ROSA)26Sor tm1$^{(CAG-tdTomato*,-EGFP*)Etes}$ (The Jackson Laboratory) reporter line. The latter mouse line expresses red fluorescent Tomato protein, along with a stop codon-blocked eGFP sequence. When Cre recombinase is

active, the sequence encoding red fluorescent Tomato protein is excised, along with the stop codon that blocks eGFP expression. As a result, cells with an active Cx3cr1 promoter at the time of tamoxifen injection will express eGFP, whereas other cells maintain the expression of red fluorescent Tomato protein. To avoid contamination with maternal macrophages, we used mothers that were lacking Cre recombinase, and thus the maternal macrophages remained fluorescent red. Both mouse lines were kindly provided by Dr. Bernd Baumann and Prof. Dr. Jan Tuckermann (University of Ulm, Germany).

To measure ATM proliferation, and to characterize CX_3CR1^+ ATMs, we used C57/BL6 male mice at age postnatal day 7 and 56 (The Jackson Laboratory). All mouse strains were kept under specific pathogen-free conditions and experiments were carried out according to local legislation.

Organ imaging, histology and electron microscopy

Dissected fat bodies and developing tadpoles were photographed with a Nikon digital camera assembled onto a white lightbox. For hematoxylin and eosin (H&E) staining, ACP and peroxidase enzyme histochemistry, fat body samples were fixed in 4% paraformaldehyde (PFA) in phosphate buffered saline (PBS) for 24 h, paraffin embedded, sectioned and stained as described [47, 82] For TEM, fat body specimens, pancreas, or cells isolated from the fat body were fixed in 4:1 mixture of 4% PFA and concentrated glutaraldehyde, and processed as described [47]. For imaging *lurp*:eGFP$^+$ and *scl*:eGFP$^+$ cells, fat bodies, spleen and liver of tadpoles or adult specimens were cryosectioned. Briefly, tissues were fixed in 4% PFA overnight, immersed in a 10% sucrose solution in PBS overnight, embedded, frozen in Surgipath embedding medium (Leica Biosystems, Wetzlar, Germany) and sectioned using a Leica cryostat (Leica Biosystems) at 7–10 μm thickness. The eGFP signal was photographed with a Leica fluorescent microscope, using DAPI as a counterstain in Vectashield Mounting Medium (Vector Laboratories, Peterborough, UK).

For immunostaining of neuropeptide FF, we used cryosections, and used a primary antibody from Abcam (Cambridge, UK). Transmitter vesicles were labeled with an antibody raised against synaptic vesicle protein 2 (SV2, Developmental Studies Hybridoma Bank, Iowa, USA). Non-specific binding of the primary antibodies was reduced by pre-incubation of the cryosections with 1% normal goat serum for 2 h. The sections were incubated with the primary antibodies overnight. This was followed by a 2-h incubation with fluorescent secondary antibodies, and counterstaining with DAPI-containing Vectashield. CX3CR1 was detected on cryosections of mouse WAT using an antibody from Abcam (see Supplemental Table 4). Cell contours were labeled with fluorescent phalloidin (Sigma-Aldrich).

To assess BM development, we used developing hindlimbs of tadpoles, and developed femurs of adult frogs. The organs were fixed with 4% PFA overnight. Mineralized adult femurs were decalcified with 10% EDTA at 37°C. Specimens were embedded in paraffin and processed for sectioning, followed by H&E or ACP staining.

Isolation of stromal cells of the *Xenopus* fat body

Stromal cells of *Xenopus* fat body specimens were separated from adipocytes using collagenase digestion as described for ATM isolation from mouse fat depots [70]. Adipocytes were used for RNA extraction. ATMs were suspended in selection medium, consisting of 2 mM EDTA and 0.5% bovine serum albumin (BSA) in PBS, pH 7.4. Cell density was adjusted to 10^6 cells/ml and analysis was performed on a Becton Dickinson LSR II Cytometer (BD Bioscience, Franklin Lakes, New Jersey, USA). Size and intracellular complexity was assessed using FSC-A and SSC-A parameters of the cell populations. The identified cell populations (RBCs, ATMs, lymphocyte-like cells) were retrieved with preparative cell sorting using a FACS Aria Cell sorter (BD Bioscience). Sorted cells were collected for further analysis by TEM or RNA extraction. ATMs were also collected for further *in vitro* culture, as described below. Results of the FACS analyses are deposited in Flow Repository, to allow secondary use.

In vitro culture of *Xenopus* ATMs

ATMs were suspended in FACS selection medium consisting of 2 mM EDTA and 0.5% BSA in PBS (pH 7.4), and were allowed to adhere to 6-well plates in RPMI-1640 medium with 10% heat inactivated fetal calf serum. The cells were maintained at 23°C in sterile cell culture hoods under 5% CO_2.

To measure phagocytosis activity, fluorescently-labeled latex beads or non-conjugated latex beads (Sigma-Aldrich) were added to the cultures at a ratio of 1:5 (macrophage:latex bead) and incubated at 23°C for 4 h. Macrophages were harvested by trypsinization, washed with FACS selection medium and processed for FACS analysis. To detect the phagocytosed beads by microscopy, we cultured macrophages on glass bottom culture plates (Cell View slides, Greiner Bio-One, Germany). As a negative control, we used ATMs without added beads. After the phagocytosis assay, ATMs were fixed with 4% PFA for 20 min, the nuclei were stained with DAPI-containing Vectashield and analysis was carried out using a Leica fluorescent microscope. Using the same Leica microscope, we captured images sequence of the phagocytosis process in living ATM cultures using a differential interference contrast objective.

For activation of ATMs, the cultures were treated with PBS as vehicle, or with 100 ng/ml LPS from *E. coli* or 5 µg/ml pI:pC (both from Sigma-Aldrich) or with 1 nM synthetic neuropeptide FF (Phoenix Pharmaceuticals, Burlingame, California, USA).

To assay colony formation of fat body stromal cells, we used a soft agar colony-forming assay as described for *Xenopus* hematopoietic colonies [23]. Briefly, cells were suspended in 0.5% agarose dissolved in Dulbecco´s modified Eagle´s medium (DMEM), and seeded on the surface of a 1% agarose layer made with DMEM. The semi-solid agarose layers were covered with DMEM, and incubated at 23°C in sterile cell culture hoods under 5% CO_2. Colonies were collected for TEM or were photographed *in situ* using a wide-field Leica microscope with a differential interference contrast objective.

To measure proliferation, stromal cells were cultured with 0.1 mg/ml BrdU (Sigma-Aldrich) for various durations in 6-well culture dishes. The cells were collected for FACS analysis by trypsinization, fixed with 4% PFA for 20 min, and incorporated BrdU was detected with a PE-conjugated anti-BrdU antibody (BU20A; Affymetrix eBioscience, San Diego, California, USA). As negative controls, we used vehicle treated cells and BrdU-pulsed cells incubated with isotype controls.

Isolation and FACS analysis of mouse ATMs

We collected epididymal WAT (eWAT) from adult (postnatal day 56) C57/BL6 mice; tissues were pooled from 3–5 animals and ATMs were isolated using collagenase digestion as described [70]. The same technique was used to isolated SCs and ATMs from BAT and iWAT of mice at postnatal day 7 or 56. In the case of young mice (postnatal day 7), we pooled tissue samples from 12–18 animals. Cell density was adjusted to 10^6 cells/ml in selection medium (the same as that used for the analysis of *Xenopus* ATMs) and analysis was performed on a BD LSR II Cytometer (BD Bioscience). Staining was performed after fixing the cells with 4% PFA for 20 min. We incubated the cells with Fc-blocker antibody followed by fluorescent antibodies or with matching isotype controls for 2 h, as described [47]. After a 2-h incubation, the cells were washed in selection buffer and used for analysis. The used antibodies are listed in Supplemental Table 4.

RNA extraction and quantitative polymerase chain reaction

Total RNA was isolated with TRI Reagent (Sigma-Aldrich). Integrity of the RNA was evaluated by denaturing agarose gel electrophoresis. Only non-degraded RNA samples were used for cDNA synthesis, as described [83]. We used the Viia7 qPCR platform (Thermo Fischer Scientific, Waltham, USA) for analysis, and gene expression values were expressed as relative mRNA level based on the DCT and DDCT methods, using *Bactin* and *Ppia/Cypa* as

559 reference genes for mouse, and *bactin* and *gapdh* as reference genes for *Xenopus*. Primer
560 sequences are provided in Supplemental Table 5.
561
562 **Whole body irradiation and bone marrow chimerism in mouse**
563 As recipients, we used 8–10-week-old CD45.1$^+$ C57BL/6 mice (The Jackson Laboratory).
564 They were placed in a restrainer to ensure immobility during γ-irradiation. We applied a 10.5
565 Gy single dose of irradiation. Donor BM from CD45.2 allele-bearing C57BL/6 mice (The
566 Jackson Laboratory) was harvested by flushing the femur BM under sterile conditions, and
567 lineage negative CD45.2$^+$ BM cells were injected intravenously at 400 $\times 10^3$ cells/recipient
568 density. As competitor cells, we injected the equal amount of lineage-negative cells from
569 CD45.1$^+$ BM. The amount of CD45.1$^+$ and CD45.2$^+$ leukocytes in BM, peripheral blood and
570 the amount of CD45.1$^+$, F4/80$^+$ and CD45.2$^+$, F4/80$^+$ ATMs was measured by FACS 20
571 weeks after BM transplantation.
572
573 **Statistical analysis**
574 All results are expressed as the mean±s.e.m. The 2-tailed Student's unpaired t-test, or a one-
575 way analysis of variance with Dunnett's *post hoc* test was used for statistical analysis, and a
576 p-value <0.05 was considered significant. Statistical analyses were performed using the
577 GraphPad Prism 5 software package (GraphPad Prism Software Inc., La Jolla, California,
578 USA).

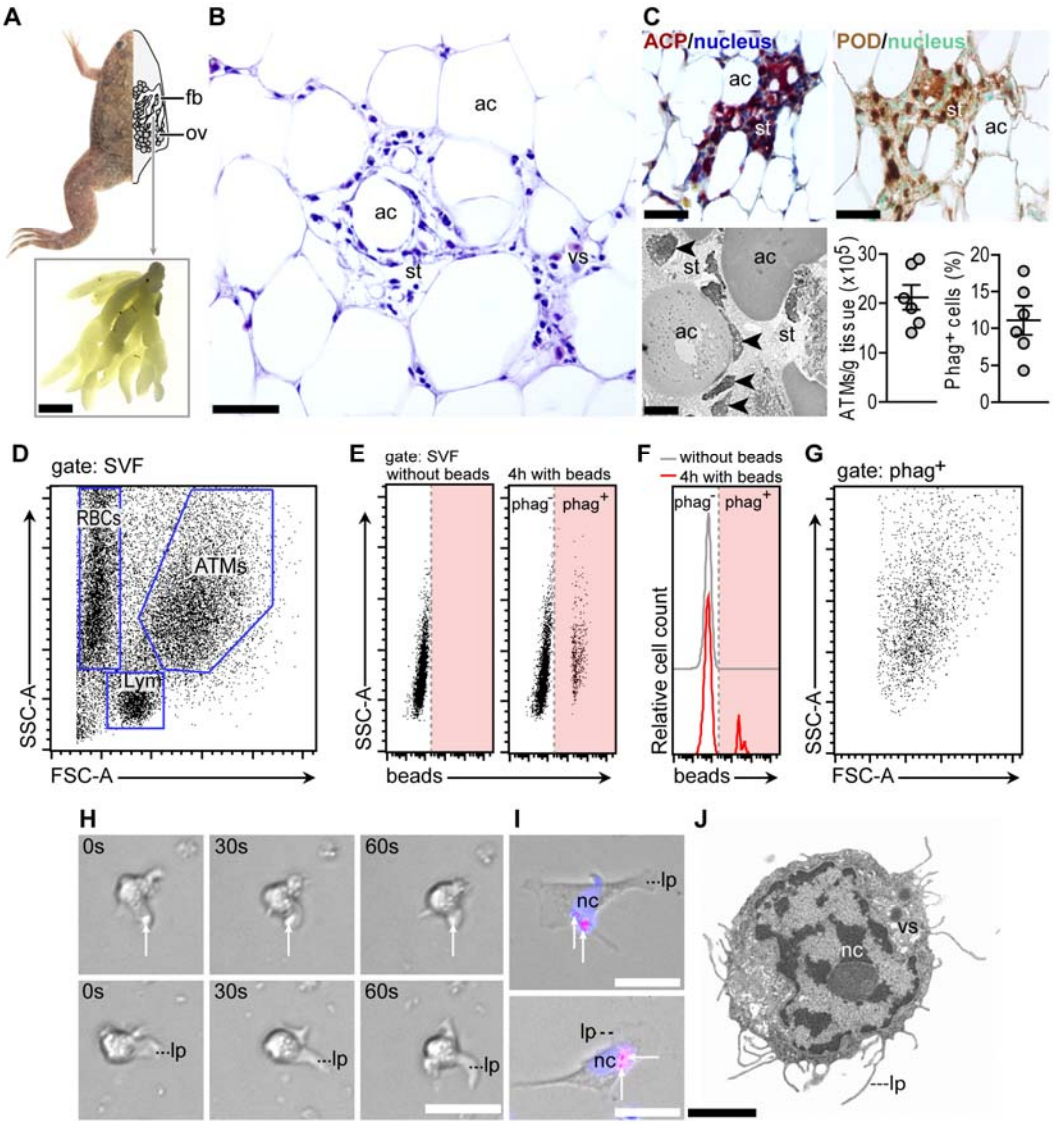

Figure 1. Adipose tissue macrophages in *Xenopus laevis*

(**A**) Anatomy of the visceral fat depot: fb, fat body; ov, ovary. Scale bar 1 cm. (**B**) Histologic assessment of the fat body by hematoxylin & eosin staining: ac, adipocyte; st, stroma; ves, blood vessel; scale bar 100 µm. (**C**) Enzyme histochemistry and ultrastructure of the fat body stroma, and quantification of ATMs. *Top*: acidic phosphatase (ACP) and peroxidase (POD) positive cells in the fat body: ac, adipocyte; st, stroma. Scale bar 50 µm. *Bottom left*: transmission electron microscopy (TEM) image of the fat body: ac, adipocyte; st, stroma; arrowheads indicate adipose tissue macrophages (ATMs; leukocytes with abundant endocytic vesicles). Scale bar 1 µm. *Bottom right*: ATM content and percentage of phagocytosing ($phag^+$) cells in the stroma. The raw data set is available at Flow Repository under accession number FR-FCM-ZYZF. (**D**) FACS analysis of SCs, stromal cells; RBCs, red blood cells; ATMs, adipose tissue macrophages; Lym, lymphocytes. For TEM images of the sorted RBCs ATMs and Lym, and for further details of the FACS analysis, see Supplemental Figure 1A–D. (**E**–**G**) Identification of phagocytosing cells in the adipose tissue stroma. The isolated SCs were incubated *in vitro* with fluorescent latex beads for 4 h: $phag^-$, cells without phagocytosed beads; $phag^+$, cells with phgocytosed beads. (**H**) Time-lapse sequence of a phagocytosing ATM. The entire time lapse sequence is shown as Supplemental Video File. Scale bar 25 µm. (**I**) ATMs with ingested fluorescent latex beads (arrows); nc, nucleus. Scale bar 15 µm. (**J**) TEM images of ATMs: nc, nucleus; lp, lamellipodia; vs, vesicles. Scale bar 1 µm. Further TEM images of ATMs are shown in Supplemental Figure 1A.

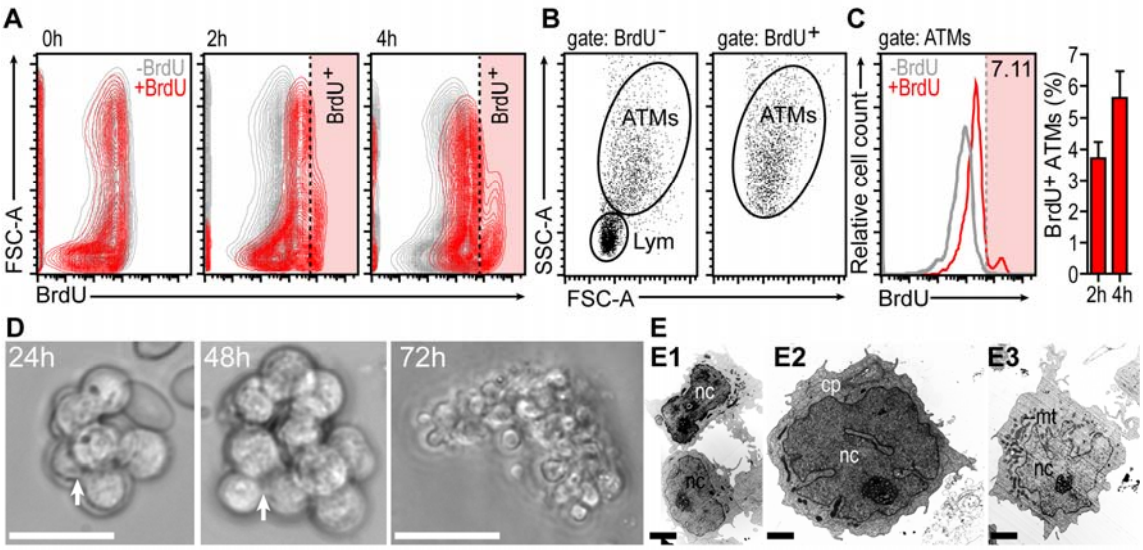

600
601 **Figure 2. Self-renewal of ATMs in *Xenopus laevis***

602 (**A**) Isolated stromal cells were cultured *in vitro* and labeled with BrdU (indicated in red),
603 n=6. In the control experiment, cells were incubated with vehicle only (indicated in gray).
604 Presence of $BrdU^+$ cells was detected by FACS. The raw data set is available in Flow
605 Repository under accession number FR-FCM-ZYZG. (**B**) Characterization of $BrdU^+$ cells
606 with FACS: ATMs, adipose tissue macrophages; Lym, lymphocytes. (**C**) Amount of $BrdU^+$
607 ATMs after 2–4 h incubation with BrdU. The histogram shows BrdU labeling after 4 h, n=3.
608 (**D**) Stromal cells were cultured *in vitro* in soft agar. Colonies formed by SCs were detected
609 after 24, 48 and 72 h. Arrow denotes cell-cell attachment site. Scale bar 50 µm. (**E**) TEM
610 images of SC colonies formed in soft agar: nc, nucleus; cp, cytoplasm. Scale bar 0.5 µm.
611

612

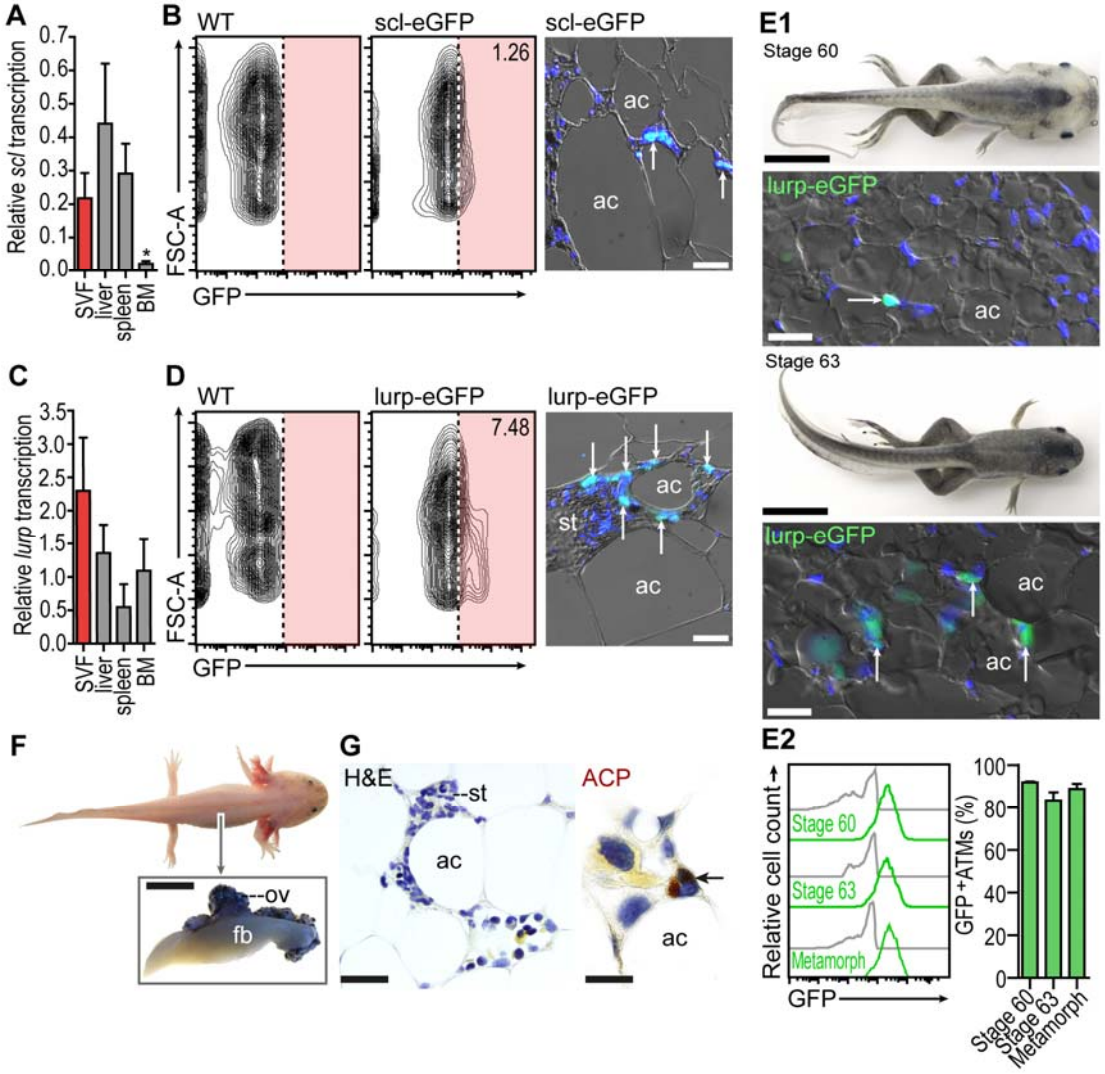

Figure 3. Development of ATMs in *Xenopus laevis*

(**A**) Relative transcription of the hematopoietic marker *scl* in stromal cells (SCs) of the fat bodies and in various hematopoietic tissues, n=6, $p<0.05$, Student´s 2-tailed, unpaired t-test. (**B**) Analysis of *scl*:eGFP$^+$ cells in adult fat bodies using FACS and histology, n=3. Arrows show *scl*:eGFP$^+$ cells; ac, adipocyte. Scale bar 50 µm. Further details are shown in Supplemental Figure 2. (**C**) Relative transcription of the macrophage precursor marker *lurp* in SCs of the adult fat bodies and in various hematopoietic tissues, n=6. (**D**) Analysis of *lurp*:eGFP$^+$ cells in adult fat bodies using FACS and histology, n=3. Arrows show *lurp*:eGFP$^+$ cells; ac, adipocyte. Scale bar 50 µm. Further details are shown in Supplemental Figure 2. (**E1**) Presence of *lurp*:eGFP$^+$ cells in developing fat bodies. Arrows show *lurp*:eGFP$^+$ cells; ac, adipocyte. Scale bars 1 cm (in macroscopic images showing developing tadpoles) and 50 µm (for the histology images). (**E2**) FACS analysis of *lurp*:eGFP$^+$ ATMs at various developmental stages, n=5 each stage. The data set is available in Flow Repository under accession number FR-FCM-ZYZE. (**F**) Anatomy of the fat body in *Ambystoma mexicanum*: fb, fat body; ov, ovary. Scale bar 1 cm. (**G**) Hematoxylin & eosin (H&E) stained section and ACP enzyme histochemistry of the fat body. Arrow shows an ACP$^+$ cell; ac, adipocyte; st, stroma. Scale bar 50 µm.

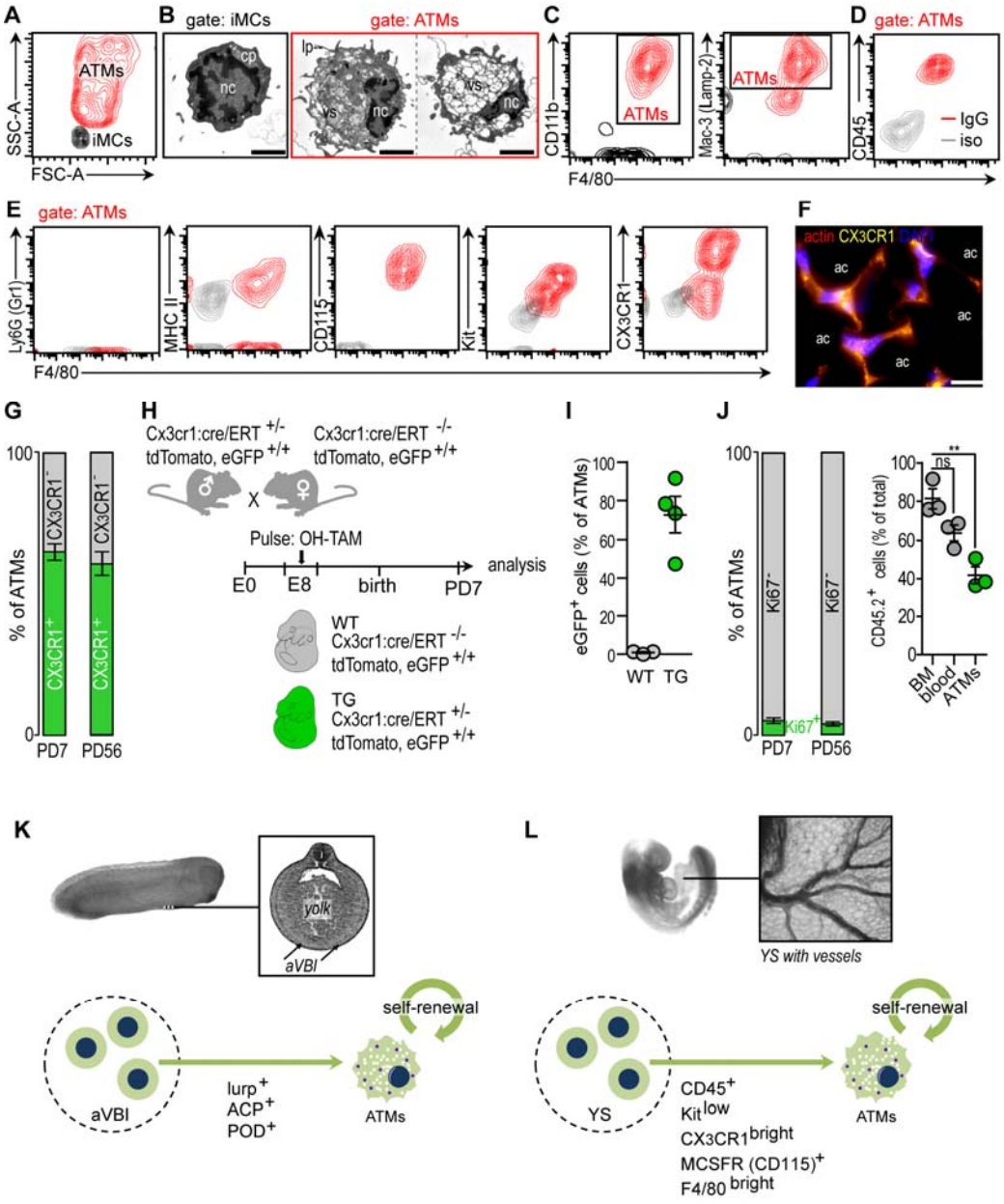

Figure 4. Homology of *Xenopus* and mouse ATM development

(**A**) FACS analysis of mouse stromal cells (SCs) isolated from the inguinal (i) WAT at postnatal day (PD)7: ATMs, adipose tissue macrophages; iMCs, immature myeloid cells. Representative of 3 independent assays. Details of FACS analysis of ATMs have been described previously [47]. (**B**) TEM images of sorted cells of the iWAT stroma at PD7: nc, nucleus; vs, vesicles; lp, lamellipoda. Scale bar 1 μm. (**C**) Identification of ATMs based on CD11b, F4/80 antigen and lysosomal protein Mac-3/Lamp-2 expression. Cells were isolated from iWAT at PD7. (**D**,**E**) Characterization of ATMs of the iWAT at PD7. (**F**) Immunohistochemistry against CX_3CR1 in iWAT at PD7. F-actin was labeled with fluorescent phalloidin. (**G**) Percentage of CX_3CR1^+ ATMs in the iWAT at PD7 and PD56. (**H**) Scheme for labeling YS-derived macrophages in the mouse. (**I**) Percentage of YS-derived (CX_3CR1-eGFP$^+$) ATMs in wild-type (WT) and transgenic (TG) iWAT at PD7. Flow Repository accession number FR-FCM-ZYZW. (**J**) Percentage of Ki67$^+$ ATMs in the iWAT at PD7 and PD56, pooled data from 3 assays, and amount of CD45.2$^+$ leukocytes in BM and blood and eWAT ATMs, 20 weeks after BM transplantation; n=3. Flow Repository accession number FR-FCM-ZYZW. (**K**,**L**) Scheme of the proposed homology of ATM development in *Xenopus* and mouse.

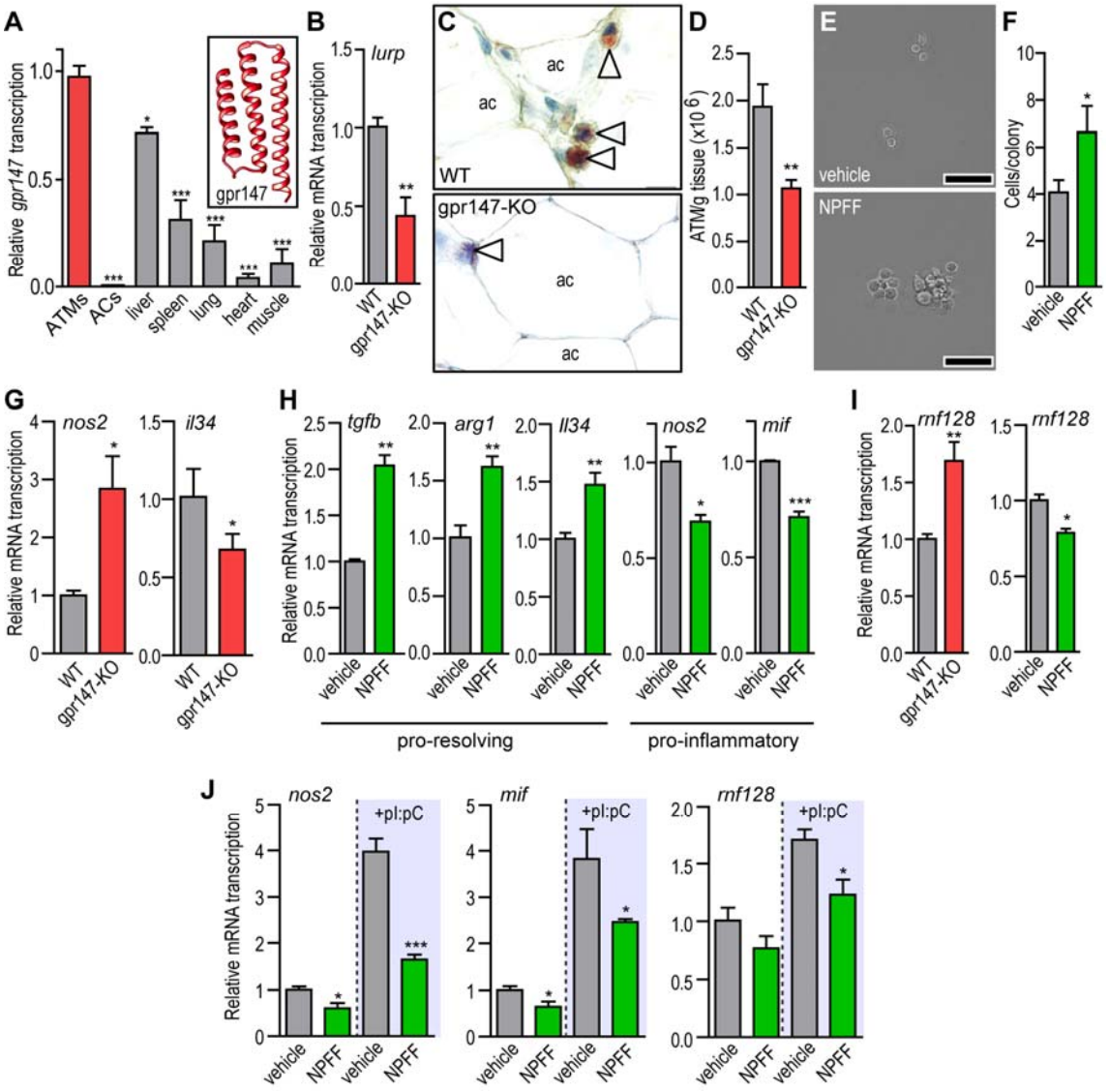

651
652 **Figure 5. Control of ATM number and activation state by gpr147 and neuropeptide FF**
653 (**A**) Relative transcription of *gpr147* mRNA in ATMs, adipocytes (ACs) and various tissues,
654 n=4. Transcript levels are normalized to ATMs. Insert shows predicted primary structure of
655 *Xenopus* gpr147 using LOMETS structure prediction software [84]. (**B**) Transcription of *lurp*
656 in wild-type (WT) and gpr147-KO fat body, n=5. (**C**) ACP^{+} cells (arrowhead) in fat body of
657 WT and gpr147-KO adult frog; ac, adipocyte. Scale bar 50 µm. (**D**) Number of ATMs
658 isolated from WT and gpr147-KO fat bodies of adult frogs, n=5. (**E**) Representative images of
659 stromal cells of a WT frog cultured in soft agar and treated with vehicle or 0.5 nM NPFF.
660 Colonies were photographed at day 3 of treatment. (**F**) Size of vehicle- or NPFF-treated
661 colonies (n>80 each assay), pooled data of 3 assays. (**G**) Relative transcription of macrophage
662 activation genes in ATMs of WT and gpr147-KO frogs, n=5. (**H**) *Xenopus* ATMs were
663 treated with vehicle or 1 nM NPFF for 1 h *in vitro* and relative transcription of macrophage
664 activation genes was measured, n=3. (**I**) Relative transcription of *rnf128* in WT and npffr1-
665 KO ATMs (n=5), and in ATMs treated *in vitro* with vehicle or 1 nM NPFF for 1 h (n=3). (**J**)
666 Relative transcription of macrophage activation genes in ATMs of *in vitro* cultured *Xenopus*
667 ATMs, treated with vehicle, 1 nM NPFF, pI:pC or the combination of pI:pC and NPFF for 4 h
668 (n=3). *p<0.05, **p<0.01, ***p<0.001, Student's t-test (B–I), or one-way ANOVA with
669 Dunnett's post-hoc test (A, J).

References

1. Rosen, E. D. and Spiegelman, B. M. (2014) What we talk about when we talk about fat. Cell 156, 20-44.
2. Boutens, L. and Stienstra, R. (2016) Adipose tissue macrophages: going off track during obesity. Diabetologia 59, 879-94.
3. Osborn, O. and Olefsky, J. M. (2012) The cellular and signaling networks linking the immune system and metabolism in disease. Nat Med 18, 363-74.
4. Qiu, Y., Nguyen, K. D., Odegaard, J. I., Cui, X., Tian, X., Locksley, R. M., Palmiter, R. D., Chawla, A. (2014) Eosinophils and type 2 cytokine signaling in macrophages orchestrate development of functional beige fat. Cell 157, 1292-308.
5. Lawrence, T. and Natoli, G. (2011) Transcriptional regulation of macrophage polarization: enabling diversity with identity. Nature reviews. Immunology 11, 750-61.
6. Amano, S. U., Cohen, J. L., Vangala, P., Tencerova, M., Nicoloro, S. M., Yawe, J. C., Shen, Y., Czech, M. P., Aouadi, M. (2014) Local proliferation of macrophages contributes to obesity-associated adipose tissue inflammation. Cell metabolism 19, 162-71.
7. Lumeng, C. N., Bodzin, J. L., Saltiel, A. R. (2007) Obesity induces a phenotypic switch in adipose tissue macrophage polarization. The Journal of clinical investigation 117, 175-84.
8. Lee, B. C. and Lee, J. (2014) Cellular and molecular players in adipose tissue inflammation in the development of obesity-induced insulin resistance. Biochimica et biophysica acta 1842, 446-62.
9. Scott, C. L., Zheng, F., De Baetselier, P., Martens, L., Saeys, Y., De Prijck, S., Lippens, S., Abels, C., Schoonooghe, S., Raes, G., Devoogdt, N., Lambrecht, B. N., Beschin, A., Guilliams, M. (2016) Bone marrow-derived monocytes give rise to self-renewing and fully differentiated Kupffer cells. Nature communications 7, 10321.

10. Ensan, S., Li, A., Besla, R., Degousee, N., Cosme, J., Roufaiel, M., Shikatani, E. A., El-Maklizi, M., Williams, J. W., Robins, L., Li, C., Lewis, B., Yun, T. J., Lee, J. S., Wieghofer, P., Khattar, R., Farrokhi, K., Byrne, J., Ouzounian, M., Zavitz, C. C., Levy, G. A., Bauer, C. M., Libby, P., Husain, M., Swirski, F. K., Cheong, C., Prinz, M., Hilgendorf, I., Randolph, G. J., Epelman, S., Gramolini, A. O., Cybulsky, M. I., Rubin, B. B., Robbins, C. S. (2016) Self-renewing resident arterial macrophages arise from embryonic CX3CR1(+) precursors and circulating monocytes immediately after birth. Nature immunology 17, 159-68.

11. Molawi, K., Wolf, Y., Kandalla, P. K., Favret, J., Hagemeyer, N., Frenzel, K., Pinto, A. R., Klapproth, K., Henri, S., Malissen, B., Rodewald, H. R., Rosenthal, N. A., Bajenoff, M., Prinz, M., Jung, S., Sieweke, M. H. (2014) Progressive replacement of embryo-derived cardiac macrophages with age. The Journal of experimental medicine 211, 2151-8.

12. Soucie, E. L., Weng, Z., Geirsdottir, L., Molawi, K., Maurizio, J., Fenouil, R., Mossadegh-Keller, N., Gimenez, G., VanHille, L., Beniazza, M., Favret, J., Berruyer, C., Perrin, P., Hacohen, N., Andrau, J. C., Ferrier, P., Dubreuil, P., Sidow, A., Sieweke, M. H. (2016) Lineage-specific enhancers activate self-renewal genes in macrophages and embryonic stem cells. Science 351, aad5510.

13. Ottaviani, E., Malagoli, D., Franceschi, C. (2011) The evolution of the adipose tissue: a neglected enigma. General and comparative endocrinology 174, 1-4.

14. Fenoglio, C., Boncompagni, E., Fasola, M., Gandini, C., Comizzoli, S., Milanesi, G., Barni, S. (2005) Effects of environmental pollution on the liver parenchymal cells and Kupffer-melanomacrophagic cells of the frog Rana esculenta. Ecotoxicology and environmental safety 60, 259-68.

15. Gallone, A., Guida, G., Maida, I., Cicero, R. (2002) Spleen and liver pigmented macrophages of Rana esculenta L. A new melanogenic system? Pigment cell research

723 / sponsored by the European Society for Pigment Cell Research and the International
724 Pigment Cell Society 15, 32-40.
725 16. Morales, H. D., Abramowitz, L., Gertz, J., Sowa, J., Vogel, A., Robert, J. (2010)
726 Innate immune responses and permissiveness to ranavirus infection of peritoneal
727 leukocytes in the frog Xenopus laevis. Journal of virology 84, 4912-22.
728 17. Grayfer, L. and Robert, J. (2016) Amphibian macrophage development and antiviral
729 defenses. Developmental and comparative immunology 58, 60-7.
730 18. Grayfer, L., De Jesus Andino, F., Robert, J. (2015) Prominent amphibian (Xenopus
731 laevis) tadpole type III interferon response to the frog virus 3 ranavirus. Journal of
732 virology 89, 5072-82.
733 19. Qi, Z. T. and Nie, P. (2008) Comparative study and expression analysis of the
734 interferon gamma gene locus cytokines in Xenopus tropicalis. Immunogenetics 60,
735 699-710.
736 20. Tomiyama, S., Nakamachi, T., Uchiyama, M., Matsuda, K., Konno, N. (2015)
737 Urotensin II upregulates migration and cytokine gene expression in leukocytes of the
738 African clawed frog, Xenopus laevis. General and comparative endocrinology 216,
739 54-63.
740 21. Robert, J. and Ohta, Y. (2009) Comparative and developmental study of the immune
741 system in Xenopus. Developmental dynamics : an official publication of the American
742 Association of Anatomists 238, 1249-70.
743 22. Haase, J., Weyer, U., Immig, K., Kloting, N., Bluher, M., Eilers, J., Bechmann, I.,
744 Gericke, M. (2014) Local proliferation of macrophages in adipose tissue during
745 obesity-induced inflammation. Diabetologia 57, 562-71.
746 23. Nogawa-Kosaka, N., Sugai, T., Nagasawa, K., Tanizaki, Y., Meguro, M., Aizawa, Y.,
747 Maekawa, S., Adachi, M., Kuroki, R., Kato, T. (2011) Identification of erythroid
748 progenitors induced by erythropoietic activity in Xenopus laevis. The Journal of
749 experimental biology 214, 921-7.

24. Smith, S. J., Kotecha, S., Towers, N., Latinkic, B. V., Mohun, T. J. (2002) XPOX2-peroxidase expression and the XLURP-1 promoter reveal the site of embryonic myeloid cell development in Xenopus. Mechanisms of development 117, 173-86.
25. Ciau-Uitz, A., Pinheiro, P., Kirmizitas, A., Zuo, J., Patient, R. (2013) VEGFA-dependent and -independent pathways synergise to drive Scl expression and initiate programming of the blood stem cell lineage in Xenopus. Development 140, 2632-42.
26. Chen, X. D. and Turpen, J. B. (1995) Intraembryonic origin of hepatic hematopoiesis in Xenopus laevis. Journal of immunology 154, 2557-67.
27. Yaparla, A., Wendel, E. S., Grayfer, L. (2016) The unique myelopoiesis strategy of the amphibian Xenopus laevis. Developmental and comparative immunology 63, 136-43.
28. Lopez, D., Lin, L., Monaghan, J. R., Cogle, C. R., Bova, F. J., Maden, M., Scott, E. W. (2014) Mapping hematopoiesis in a fully regenerative vertebrate: the axolotl. Blood 124, 1232-41.
29. Balic, A., Garcia-Morales, C., Vervelde, L., Gilhooley, H., Sherman, A., Garceau, V., Gutowska, M. W., Burt, D. W., Kaiser, P., Hume, D. A., Sang, H. M. (2014) Visualisation of chicken macrophages using transgenic reporter genes: insights into the development of the avian macrophage lineage. Development 141, 3255-65.
30. Epelman, S., Lavine, K. J., Beaudin, A. E., Sojka, D. K., Carrero, J. A., Calderon, B., Brija, T., Gautier, E. L., Ivanov, S., Satpathy, A. T., Schilling, J. D., Schwendener, R., Sergin, I., Razani, B., Forsberg, E. C., Yokoyama, W. M., Unanue, E. R., Colonna, M., Randolph, G. J., Mann, D. L. (2014) Embryonic and adult-derived resident cardiac macrophages are maintained through distinct mechanisms at steady state and during inflammation. Immunity 40, 91-104.
31. Perdiguero, E. G., Klapproth, K., Schulz, C., Busch, K., Azzoni, E., Crozet, L., Garner, H., Trouillet, C., de Bruijn, M. F., Geissmann, F., Rodewald, H. R. (2014)

776 Tissue-resident macrophages originate from yolk-sac-derived erythro-myeloid
777 progenitors. Nature.
778 32. Schulz, C., Gomez Perdiguero, E., Chorro, L., Szabo-Rogers, H., Cagnard, N.,
779 Kierdorf, K., Prinz, M., Wu, B., Jacobsen, S. E., Pollard, J. W., Frampton, J., Liu, K.
780 J., Geissmann, F. (2012) A lineage of myeloid cells independent of Myb and
781 hematopoietic stem cells. Science 336, 86-90.
782 33. Yona, S., Kim, K. W., Wolf, Y., Mildner, A., Varol, D., Breker, M., Strauss-Ayali, D.,
783 Viukov, S., Guilliams, M., Misharin, A., Hume, D. A., Perlman, H., Malissen, B.,
784 Zelzer, E., Jung, S. (2013) Fate mapping reveals origins and dynamics of monocytes
785 and tissue macrophages under homeostasis. Immunity 38, 79-91.
786 34. DeFalco, T., Bhattacharya, I., Williams, A. V., Sams, D. M., Capel, B. (2014) Yolk-
787 sac-derived macrophages regulate fetal testis vascularization and morphogenesis.
788 Proceedings of the National Academy of Sciences of the United States of America
789 111, E2384-93.
790 35. Kozak, L. P. (2011) The genetics of brown adipocyte induction in white fat depots.
791 Frontiers in endocrinology 2, 64.
792 36. Waqas, S. F. H., Hoang, A. C., Lin, Y., Ampem, G., Azegrouz, H., Balogh, L.,
793 Thuróczy, J., Chen, J., Gerling, I. C., Nam, S., Lim, J., Martinez-Ibañez, J., Real, J. T.,
794 Paschke, S., Quillet, R., Ayachi, S., Simonin, F., Schneider, M., Brinkman, J.,
795 Lamming, D. W., Seroogy, C. M., Röszer, T. (2017) Neuropeptide FF increases M2
796 activation and self-renewal of adipose tissue macrophages. The Journal of clinical
797 investigation in press.
798 37. Jenkins, S. J., Ruckerl, D., Cook, P. C., Jones, L. H., Finkelman, F. D., van Rooijen,
799 N., MacDonald, A. S., Allen, J. E. (2011) Local macrophage proliferation, rather than
800 recruitment from the blood, is a signature of TH2 inflammation. Science 332, 1284-8.
801 38. Röszer, T. (2015) Understanding the Mysterious M2 Macrophage through Activation
802 Markers and Effector Mechanisms. Mediators of Inflammation 2015, 16.

803 39. Elphick, M. R. and Mirabeau, O. (2014) The Evolution and Variety of RFamide-Type
804 Neuropeptides: Insights from Deuterostomian Invertebrates. Frontiers in
805 endocrinology 5, 93.
806 40. Herrera-Herrera, M. L. and Salazar-Olivo, L. A. (2008) RFamide neuropeptides
807 inhibit murine and human adipose differentiation. Biochemical and biophysical
808 research communications 377, 29-34.
809 41. Sun, Y. L., Zhang, X. Y., Sun, T., He, N., Li, J. Y., Zhuang, Y., Zeng, Q., Yu, J.,
810 Fang, Q., Wang, R. (2013) The anti-inflammatory potential of neuropeptide FF in
811 vitro and in vivo. Peptides 47, 124-32.
812 42. Silva, A. B., Aw, D., Palmer, D. B. (2009) Neuropeptides and thymic hormones in the
813 Xenopus thymus. Frontiers in bioscience 14, 1990-2003.
814 43. Ganea, D. and Delgado, M. (2001) Inhibitory neuropeptide receptors on macrophages.
815 Microbes and infection / Institut Pasteur 3, 141-7.
816 44. Grayfer, L. and Robert, J. (2015) Distinct functional roles of amphibian (Xenopus
817 laevis) colony-stimulating factor-1- and interleukin-34-derived macrophages. Journal
818 of leukocyte biology 98, 641-9.
819 45. Sahoo, A., Alekseev, A., Obertas, L., Nurieva, R. (2014) Grail controls Th2 cell
820 development by targeting STAT6 for degradation. Nature communications 5, 4732.
821 46. Lopez, J. M., Moreno, N., Morona, R., Munoz, M., Gonzalez, A. (2006)
822 Spatiotemporal sequence of appearance of NPFF-immunoreactive structures in the
823 developing central nervous system of Xenopus laevis. Peptides 27, 1036-53.
824 47. Ampem, G., Azegrouz, H., Bacsadi, A., Balogh, L., Schmidt, S., Thuroczy, J., Roszer,
825 T. (2016) Adipose tissue macrophages in non-rodent mammals: a comparative study.
826 Cell and tissue research 363, 461-78.
827 48. Ramsay, T. G., Stoll, M. J., Blomberg le, A., Caperna, T. J. (2016) Regulation of
828 cytokine gene expression by orosomucoid in neonatal swine adipose tissue. Journal of
829 animal science and biotechnology 7, 25.

49. Westover, A. J., Johnston, K. A., Buffington, D. A., Humes, H. D. (2016) An Immunomodulatory Device Improves Insulin Resistance in Obese Porcine Model of Metabolic Syndrome. Journal of diabetes research 2016, 3486727.
50. Forbes, S. J. and Rosenthal, N. (2014) Preparing the ground for tissue regeneration: from mechanism to therapy. Nat Med 20, 857-69.
51. Godwin, J. W., Pinto, A. R., Rosenthal, N. A. (2013) Macrophages are required for adult salamander limb regeneration. Proceedings of the National Academy of Sciences of the United States of America 110, 9415-20.
52. Zammit, P. S., Clarke, J. D., Golding, J. P., Goodbrand, I. A., Tonge, D. A. (1993) Macrophage response during axonal regeneration in the axolotl central and peripheral nervous system. Neuroscience 54, 781-9.
53. Jones, J. E. and Corwin, J. T. (1996) Regeneration of sensory cells after laser ablation in the lateral line system: hair cell lineage and macrophage behavior revealed by time-lapse video microscopy. The Journal of neuroscience : the official journal of the Society for Neuroscience 16, 649-62.
54. Takahama, H., Kinoshita, T., Sasaki, F. (1992) Structural and endocytotic differences of fibroblasts and macrophages in the tail fin of amphibian larvae during metamorphosis. Archives of histology and cytology 55, 437-48.
55. Sichel, G., Scalia, M., Mondio, F., Corsaro, C. (1997) The amphibian Kupffer cells build and demolish melanosomes: an ultrastructural point of view. Pigment cell research / sponsored by the European Society for Pigment Cell Research and the International Pigment Cell Society 10, 271-87.
56. Corsaro, C., Scalia, M., Leotta, N., Mondio, F., Sichel, G. (2000) Characterisation of Kupffer cells in some Amphibia. Journal of anatomy 196 (Pt 2), 249-61.
57. Scalia, M., Di Pietro, C., Poma, M., Ragusa, M., Sichel, G., Corsaro, C. (2004) The spleen pigment cells in some amphibia. Pigment cell research / sponsored by the

European Society for Pigment Cell Research and the International Pigment Cell Society 17, 119-27.

58. Sichel, G., Scalia, M., Corsaro, C. (2002) Amphibia Kupffer cells. Microscopy research and technique 57, 477-90.

59. Kirkham, M., Berg, D. A., Simon, A. (2011) Microglia activation during neuroregeneration in the adult vertebrate brain. Neuroscience letters 497, 11-6.

60. Mills, E. A., Davis, C. H., Bushong, E. A., Boassa, D., Kim, K. Y., Ellisman, M. H., Marsh-Armstrong, N. (2015) Astrocytes phagocytose focal dystrophies from shortening myelin segments in the optic nerve of Xenopus laevis at metamorphosis. Proceedings of the National Academy of Sciences of the United States of America 112, 10509-14.

61. Yaeger, J. A. and Kraucunas, E. (1969) Fine structure of the resorptive cells in the teeth of frogs. The Anatomical record 164, 1-13.

62. Wistuba, J., Bolte, M., Clemen, G. (2000) The odontoclasts of Ambystoma mexicanum. Annals of anatomy = Anatomischer Anzeiger : official organ of the Anatomische Gesellschaft 182, 415-22.

63. Colombo, B. M., Scalvenzi, T., Benlamara, S., Pollet, N. (2015) Microbiota and mucosal immunity in amphibians. Frontiers in immunology 6, 111.

64. McCusker, C. and Gardiner, D. M. (2011) The axolotl model for regeneration and aging research: a mini-review. Gerontology 57, 565-71.

65. Paredes, R., Ishibashi, S., Borrill, R., Robert, J., Amaya, E. (2015) Xenopus: An in vivo model for imaging the inflammatory response following injury and bacterial infection. Developmental biology 408, 213-28.

66. Zambrano, L., Reidl, P., McKay, J., Griffiths, R., Shaffer, B., Flores-Villela, O., Parra-Olea, G., Wake, D. (2010) Ambystoma mexicanum. . The IUCN Red List of Threatened Species, e.T1095A3229615. .

67. Chang, Z. L. (2009) Recent development of the mononuclear phagocyte system: in memory of Metchnikoff and Ehrlich on the 100th Anniversary of the 1908 Nobel Prize in Physiology or Medicine. Biol Cell 101, 709-21.
68. Fischman, D. A. and Hay, E. D. (1962) Origin of osteoclasts from mononuclear leucocytes in regenerating newt limbs. The Anatomical record 143, 329-37.
69. Costa, R. M., Soto, X., Chen, Y., Zorn, A. M., Amaya, E. (2008) spib is required for primitive myeloid development in Xenopus. Blood 112, 2287-96.
70. Weisberg, S. P., McCann, D., Desai, M., Rosenbaum, M., Leibel, R. L., Ferrante, A. W. (2003) Obesity is associated with macrophage accumulation in adipose tissue. Journal of Clinical Investigation 112, 1796-1808.
71. Koh, Y. J., Kang, S., Lee, H. J., Choi, T. S., Lee, H. S., Cho, C. H., Koh, G. Y. (2007) Bone marrow-derived circulating progenitor cells fail to transdifferentiate into adipocytes in adult adipose tissues in mice. The Journal of clinical investigation 117, 3684-95.
72. Ablamunits, V., Weisberg, S. P., Lemieux, J. E., Combs, T. P., Klebanov, S. (2007) Reduced adiposity in ob/ob mice following total body irradiation and bone marrow transplantation. Obesity 15, 1419-29.
73. Marathe, C., Bradley, M. N., Hong, C., Chao, L., Wilpitz, D., Salazar, J., Tontonoz, P. (2009) Preserved glucose tolerance in high-fat-fed C57BL/6 mice transplanted with PPARgamma-/-, PPARdelta-/-, PPARgammadelta-/-, or LXRalphabeta-/- bone marrow. Journal of lipid research 50, 214-24.
74. Claycombe, K. J., Brissette, C. A., Ghribi, O. (2015) Epigenetics of inflammation, maternal infection, and nutrition. The Journal of nutrition 145, 1109S-1115S.
75. Wang, H., He, M., Hou, Y., Chen, S., Zhang, X., Zhang, M., Ji, X. (2016) Role of decidual CD14(+) macrophages in the homeostasis of maternal-fetal interface and the differentiation capacity of the cells during pregnancy and parturition. Placenta 38, 76-83.

76. Roger, T., Schneider, A., Weier, M., Sweep, F. C., Le Roy, D., Bernhagen, J., Calandra, T., Giannoni, E. (2016) High expression levels of macrophage migration inhibitory factor sustain the innate immune responses of neonates. Proceedings of the National Academy of Sciences of the United States of America 113, E997-1005.
77. Hubrecht, R. C. and Kirkwood, J. (2010) The UFAW Handbook on the Care and Management of Laboratory and Other Research Animals, 8th Edition. Wiley-Blackwell.
78. Faber, J. and Nieuwkoop, P. D. (1967) Normal table of Xenopus laevis (Daudin) : a systematical and chronological survey of the development from the fertilized egg till the end of metamorphosis Amsterdam: North-Holland Pub. Co.
79. Allmeling, C. (2013) Threatened Newts and Salamanders of the World - Captive Care Management MERTENSIELLA No 20 e, Mannheim 7-15.
80. Guille, M. (1999) Molecular Methods in Developmental Biology: Xenopus and Zebrafish. Humana Press.
81. Nakayama, T., Blitz, I. L., Fish, M. B., Odeleye, A. O., Manohar, S., Cho, K. W., Grainger, R. M. (2014) Cas9-based genome editing in Xenopus tropicalis. Methods in enzymology 546, 355-75.
82. Silveira, S. R. and Hadler, W. A. (1978) Catalases and peroxidases histochemical detection; techniques suitable to discriminate these enzymes. Acta histochemica 63, 1-10.
83. Röszer, T., Menendez-Gutierrez, M. P., Lefterova, M. I., Alameda, D., Nunez, V., Lazar, M. A., Fischer, T., Ricote, M. (2011) Autoimmune kidney disease and impaired engulfment of apoptotic cells in mice with macrophage peroxisome proliferator-activated receptor gamma or retinoid X receptor alpha deficiency. Journal of immunology 186, 621-31.
84. Wu, S. and Zhang, Y. (2007) LOMETS: a local meta-threading-server for protein structure prediction. Nucleic acids research 35, 3375-82.

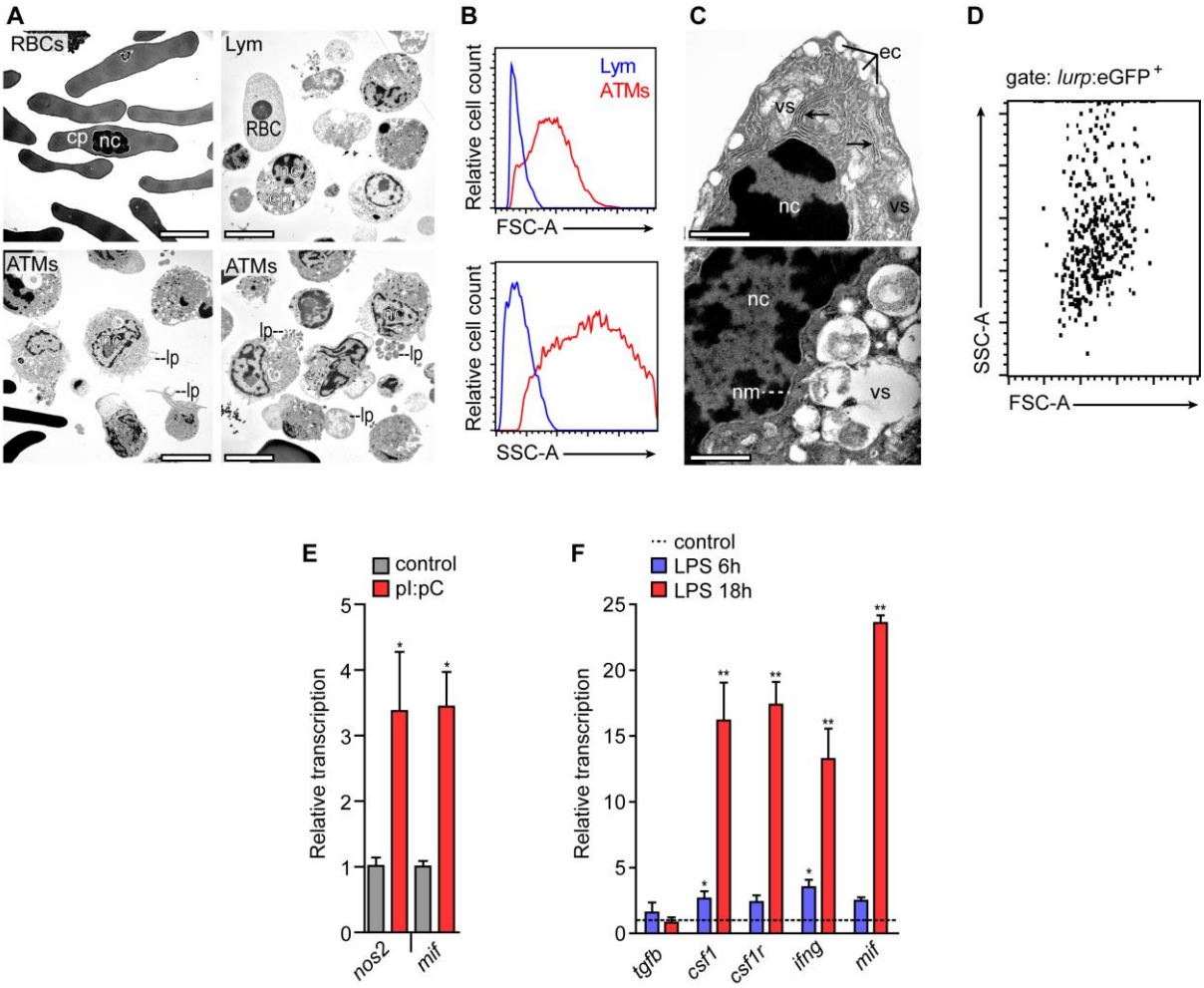

Supplemental Figure 1. Preparative cell sorting and transmission electron microscopy analysis of adipose tissue stromal cells in adult *Xenopus*. Response of *Xenopus* ATMs to pathogen-associated signals

(**A**) Transmission electron microscopy (TEM) images of cell types in the fat body stroma. Stromal cells of the fat bodies were isolated from adult *Xenopus* and used for preparative cell sorting. Three populations were defined based on their SSC-A/FSC-A characteristics, as shown in Figure 1D: RBCs, red blood cells; Lym, lymphocyte-like cells; ATMs, adipose tissue macrophages; cp, cytoplasm; nc, nucleus; lp, lamellipodia. Scale bars 10 µm. (**B**) Comparison of cell size/cell complexity of lymphocytes and ATMs using their SSC-A and FSC-A characteristics. (**C**) TEM images of the cell borders and intracellular content of ATMs: ec, endocytotic vesicle; vs, vesicle; nc, nucleus; nm, nuclear membrane. (**D**) FACS plot showing FSC-A and SSC-A characteristics of *lurp*:eGFP$^+$ stromal cells. The *lurp*:eGFP$^+$ cloud displayed similar FSC-A/SSC-A characteristics to those of ATMs (see Figure 1D). (**E**,**F**) ATMs were treated *in vitro* with pI:pC or LPS. Transcription of genes involved in immune response was measured, n=3, *p<0.01, **p<0.05, Student´s 2-tailed, unpaired t-test.

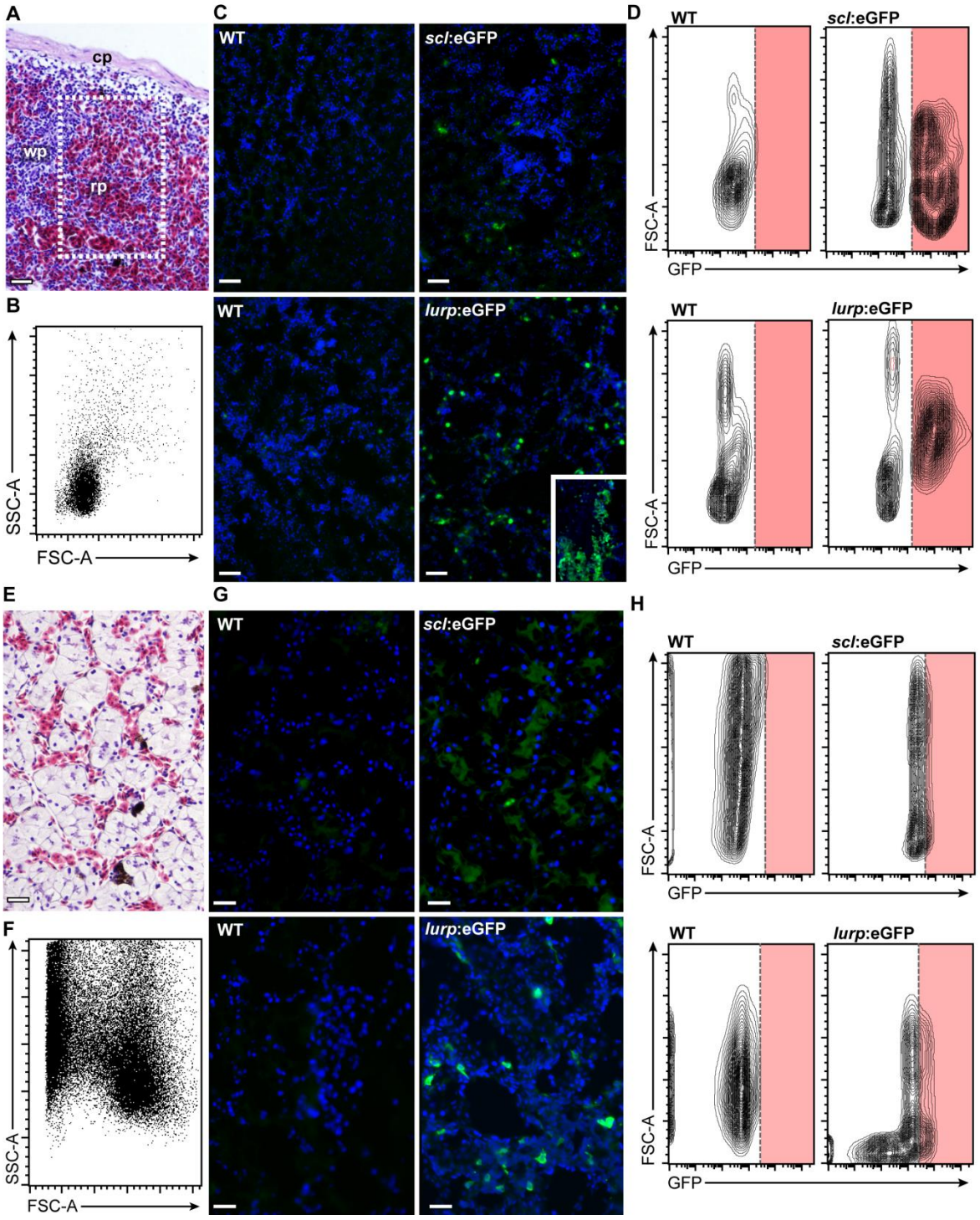

Supplemental Figure 2. Histology and FACS analysis of scl$^+$ and lurp$^+$ cells in the spleen and the liver

(**A**) Histologic assessment of the spleen by hematoxylin and eosin (H&E) staining: cp, capsule; wp, white pulp; rp, red pulp. Scale bar 100 μm. Frame indicates regions shown in panel B. (**B**) FACS plot of splenic cells. (**C**) Histology of spleen in wild-type (WT) and *scl*:eGPF or *lurp*:eGFP adult *Xenopus*. Scale bar 100 μm. Inset shows subcapsular region. (**D**) FACS analysis of eGFP$^+$ cells. (**E**) Histologic assessment of the liver by H&E staining. Scale bar 100 μm. (**F**) FACS plot of hepatic cells. (**G**) Histology of liver in WT and *scl*:eGPF or *lurp*:eGFP adult *Xenopus*. Scale bar 100 μm. (**H**) FACS analysis of eGFP$^+$ cells.

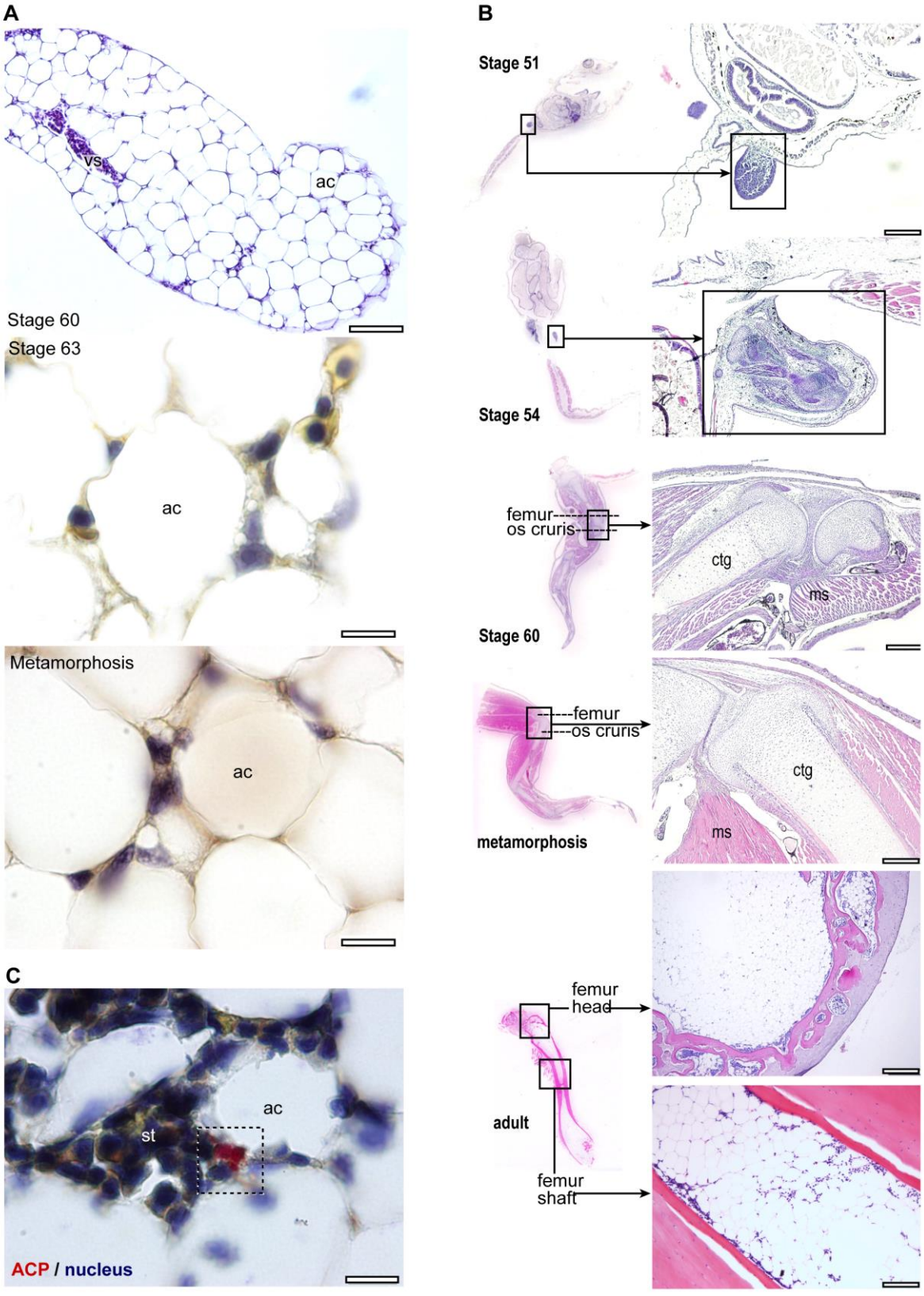

Supplemental Figure 3. Histology of the developing fat body in *Xenopus* embryo

(**A**) H&E-stained sections of the fat body from stage 60, stage 63 and metamorphosis: ac, adipocyte; vs, vessel. Scale bar 150 μm (stage 60), 10 μm (stage 63, metamorphosis). (**B**) Bone marrow development in *Xenopus* embryo. H&E-stained sections of the hindlimb at various developmental stages. Bone marrow cavity is visible in adult specimens and is filled

with adipose cells: ctg, cartilage; ms, muscle. Scale bar 200 μm. (**C**) Macrophages in the adult bone marrow of *Xenopus*. Acid phosphatase (ACP) enzymehistochemistry was used to label macrophages. The bone marrow is filled with adipocytes (ac). Stromal cells (st) can be seen among the adipocytes, including ACP^+ cells, which are highlighted with a dotted frame. Scale bar 50 μm.

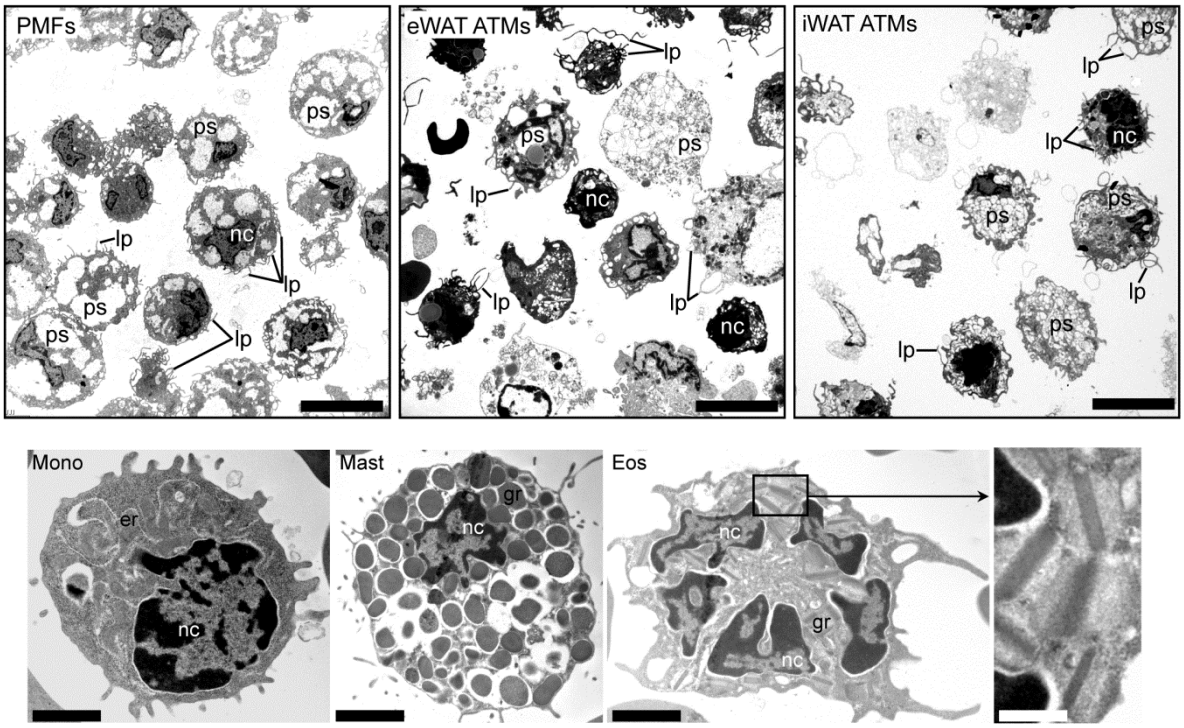

Supplemental Figure 4. Transmission electron microscopy analysis of ATMs in mouse
Top: TEM images of peritoneal macrophages (PMFs) and ATMs of the epididymal (e) WAT and the inguinal (i) WAT. ATMs were retrieved by preparative cell sorting using their FSC-A/SSC-A characteristics as described before (1). Scale bar 15 μm. *Bottom*: Leukocytes isolated from inguinal brown adipose tissue: Mono, monocyte; Mast, mastocyte; Eos, eosinophil granulocyte; nc, nucleus; lp, lamellipodia; ps, phagosome; er, endoplasmic reticule; gr, granule. Scale bar 1 μm. Scale bar in inset 0.1 μm.

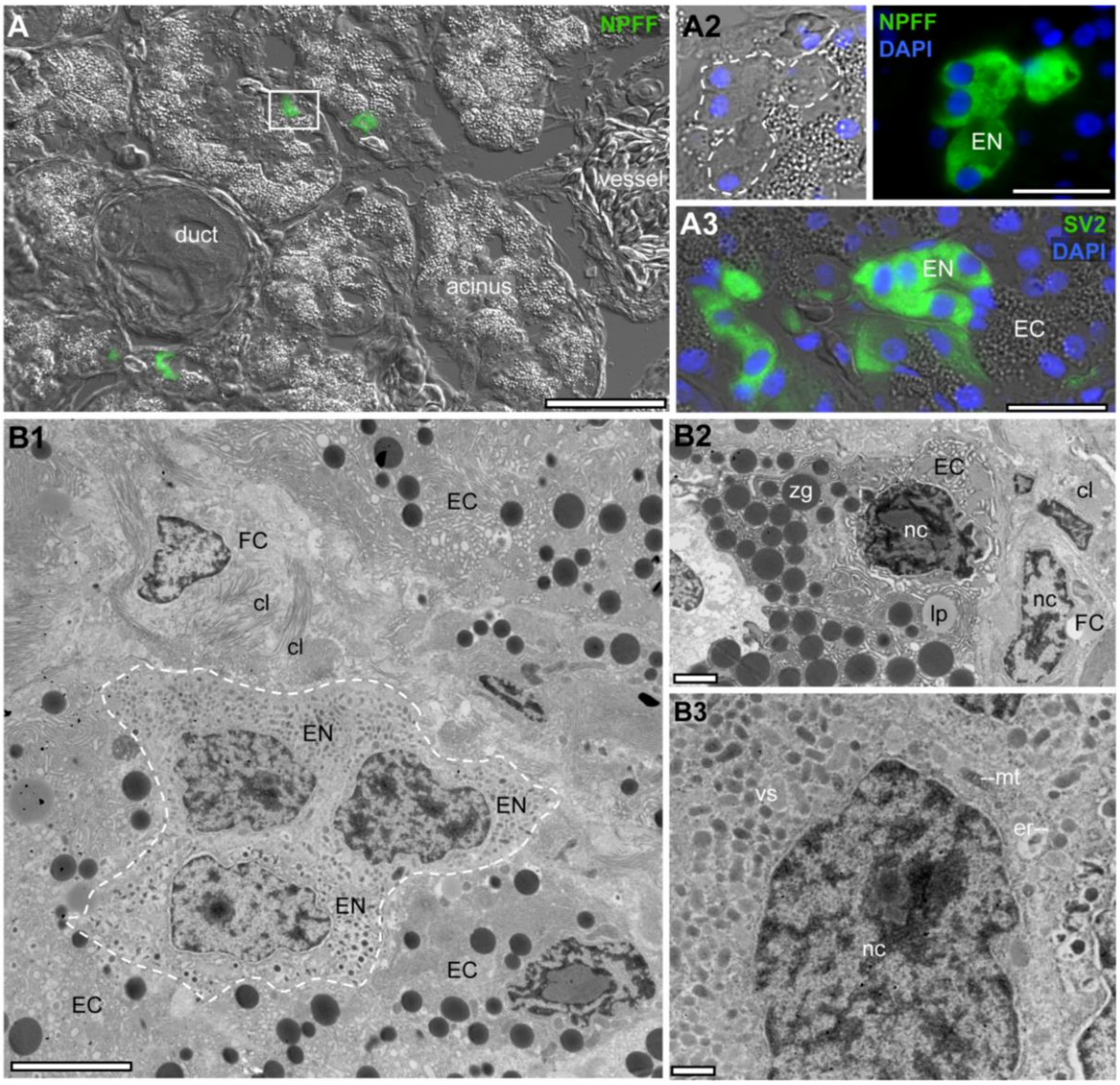

Supplemental Figure 5. Pancreatic distribution of neuropeptide-FF in adult *Xenopus laevis*

(**A**) Overview of the pancreas showing the exocrine parenchyme. Scattered endocrine cells with NPFF immunostaining are labeled with frame. Scale bar 200 µm. (**A2**) Differential interference contrast *(left)* and fluorescent *(right)* image of a group of endocrine cells (EN). Scale bar 50 µm. (**A3**) Endocrine cells stained for synaptic vesicle protein 2 (SV2). Scale bar 50 µm. (**B1**) A group of endocrine cells seen by transmission electron microscopy. EN: endocrine cells, EC: exocrine cells, FC: fibrocytes, cl: collagen fibers. Scale bar 1 µm. (**B2**) Higher magnification of an exocrine cell (EC): nc, nucleus; zg, zymogen granules; lp, lipid droplet. A fibrocyte (FC) is seen adjacent to the exocrine cells (EC): cl, collagen fibers. Scale bar 1 µm. (**B3**) Higher magnification of an endocrine cell: nc, nucleus; er, endoplasmic reticule; mt, mitochondria; vs, transmitter vesicles. Scale bar 1 µm.

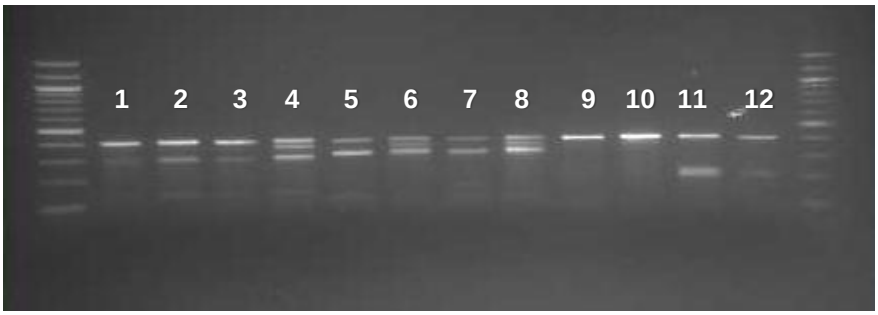

Supplemental Figure 6. T7 endonuclease I assay to detect Cas9 induced mutations

1–4 sgRNA #3+#4
5–8 sgRNA #2
9,10 control embryos
11,12 sgRNA #1

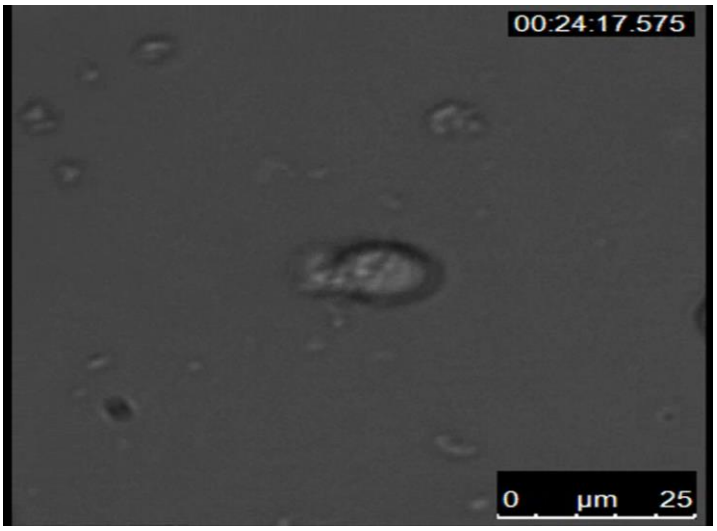

Supplemental Video File: Image sequence of a phagocytosing *Xenopus* ATM

ATMs were cultured *in vitro* and phagocytosis was recorded using a differential interference contrast Leica microscope. We used unconjugated latex beads for phagocytosis. Frame frequency was 1/minute.

Supplemental Table 1. Identification of YS-derived macrophages using specific markers	
Yolk sac stem cells with macrophage lineage commitment	**Cell markers** (2-7)
Maternal YS macrophages* E7.5-E9.5	$CD45^+$ Kit^- $CD31^-$ $Mac1^+$ $F4/80^+$
Stage 1 YS macrophages E8	$CD45^-$ Kit^+ $CD31^+$
Stage 2 YS macrophages E8-E10	$CD45^+$ Kit^+ $CD31^+$ $Mac1^+$
Stage 3 YS macrophages E8-E10	$CD45^+$ Kit^{low} $CD31^+$ $Mac1^+$ $MCSFR^+$ CX_3CR1^+
Stage 4 YS macrophages from E10.5**	$CD45^+$ Kit^{low} CX_3CR1^{bright} $MCSFR^+$ $F4/80^{bright}$
* This population disappears at E9.5, and is therefore not analyzed because of its lack of effect on postnatal macrophage progeny. ** This population persists in adult tissues and retains proliferative ability, and is thus considered a monopotent stem cell pool. CD45, leukocyte common antigen; Kit, c-kit; CD31, platelet-endothelial cell adhesion molecule [PECAM-1]; Mac1, macrophage-1 antigen; CX_3CR1, CX3C chemokine receptor-1; MCSFR, macrophage colony stimulating factor receptor; F4/80, murine macrophage marker	

Supplemental Table 2. Oligonucleotides used to prepare sgRNA templates	
#1	taatacgactcactata**GGGCATGATTGGCAATATGT**gttttagagctagaa
#2	taatacgactcactata**GGGTTGTCCACTAAAGTGGT**gttttagagctagaa
#3	taatacgactcactata**GGAATCAGCGACTTGCTGGT**gttttagagctagaa
#4	taatacgactcactata**GGCAGTCAGCGACTTGCTGG**gttttagagctagaa

Supplemental Table 3. Primer sequences used in evaluation of gene targeting efficiency in sgRNA/Cas9-injected *X. laevis* embryos	
X.l chr7S npffr1 fw	5' CCTTCCTTGAAATGTTACTCTGG
X.l chr7S npffr1 rev	5' TAAAGAAGCCACTGTCCTTCAGTC
X.l chr7L npffr1 fw	5' TGAAACCTTCCTTGTTACTCCAGC
X.l chr7L npffr1 rev	5' TGCCACTGTTCTTCAGTTCTC

Supplemental Table 4. List of antibodies used in FACS analysis	
Antigen, conjugate	**Commercial source, reference of clone number**
Fc-receptor blocker	BD Biosciences, 553141
mouse Ki67, PE Cy7	Affymetrix eBioscience, SolA15
mouse MHC-II, AF700	Affymetrix eBioscience, MS/114.15.2
mouse Gr-1 (Ly6G), PE or PECy7	Affymetrix eBioscience, RB6-805 or RB6-8C5
mouse CD45, PeCy5.5 or APC, CD45.1 APC, CD45.2 AF700	Affymetrix eBioscience, 30-F11, 30-F11, 17-0453-81, 56-0454-81
BrdU, PE	Affymetrix eBioscience, BU20A
mouse CD11b, APC or AF700	Affymetrix eBioscience, M1/70
mouse Kit (c-kit), PE	Affymetrix eBioscience, 2B8
mouse CD115 (MCSFR), PECy7	Affymetrix eBioscience, AFS98
mouse Mac-3 (Lamp-2), PE	BD Pharmingen, 553324
mouse F4/80, APC or PE	Affymetrix eBioscience, BM8, 12-4801-80
mouse/human CX_3CR1, unconjugated	Abcam, Cambridge, UK, ref. no. ab8021, rabbit polyclonal
secondary antibody	donkey anti rabbit AF488, Life Technologies

Supplemental Table 5. Primer sequences used in qPCR analysis		
bactin	fw	CCATTGGTAACGAGCGTTT
	rev	GAGGGGCCAGACTCATCATA
gapdh	fw	GACATCAAGGCCGCCATTAAGACT
	rev	AGATGGAGGAGTGAGTGTCACCAT
lurp	fw	CGGTGCTGTTCTACTGACCT
	rev	GGGGTCTTTGCGTGGTTCTT
scl	fw	CAAACTTCTCGATGACCAGG
	rev	GCTTGATGGAGATTTCTGCTG
arg1	fw	CTTACAATGAGTAGCCAAGG
	rev	GCAGAGAAAATGAGGATTCG
nos2	fw	AGCCCCACACAACACAGAAA
	rev	AAAGTTACCTAAGCCCCGCC
ifng	fw	CTGAGGAAATACTTTAACTCCATTGACC
	rev	TTGTAACATCTCCCACCTGTATTGTC
mif	fw	CCAGCTGAGTACATTGCAATTC
	rev	CCCTATCTTTCCAATGCTGC
csf1r	fw	GGCCTCAGCGCGCTTATATGTCAA
	rev	AAGCAGGGTAGAGTGGCATCTTTG
csf1	fw	ATCGAACTCTGTCCAAGCTGGATG
	rev	GGACGAAGCAAGCATCTGCCTTAT
tgfb	fw	CAAACTGCTGTGTGAAACCTC
	rev	CTGTACCATGTCTTTGCTTTGC
il34	fw	AATCAGTTCGTCCCAAGGCA
	rev	TCTTCCCTATTACCAGCATCGC
rnf128	fw	CCAATGCTTCCCCTTACCCT
	rev	TTGTCTTTGCAGGCGGTGTA

References

1. Ampem G, Azegrouz H, Bacsadi A, Balogh L, Schmidt S, Thuroczy J, and Roszer T. Adipose tissue macrophages in non-rodent mammals: a comparative study. *Cell and tissue research.* 2016;363(2):461-78.
2. Schulz C, Gomez Perdiguero E, Chorro L, Szabo-Rogers H, Cagnard N, Kierdorf K, Prinz M, Wu B, Jacobsen SE, Pollard JW, et al. A lineage of myeloid cells independent of Myb and hematopoietic stem cells. *Science.* 2012;336(6077):86-90.
3. Bertrand JY, Jalil A, Klaine M, Jung S, Cumano A, and Godin I. Three pathways to mature macrophages in the early mouse yolk sac. *Blood.* 2005;106(9):3004-11.
4. Lichanska AM, Browne CM, Henkel GW, Murphy KM, Ostrowski MC, McKercher SR, Maki RA, and Hume DA. Differentiation of the mononuclear phagocyte system during mouse embryogenesis: the role of transcription factor PU.1. *Blood.* 1999;94(1):127-38.
5. Lichanska AM, and Hume DA. Origins and functions of phagocytes in the embryo. *Experimental hematology.* 2000;28(6):601-11.
6. Fennie C, Cheng J, Dowbenko D, Young P, and Lasky LA. CD34+ endothelial cell lines derived from murine yolk sac induce the proliferation and differentiation of yolk sac CD34+ hematopoietic progenitors. *Blood.* 1995;86(12):4454-67.
7. Yoder MC. Generation of HSCs in the embryo and assays to detect them. *Oncogene.* 2004;23(43):7161-3.